CrossMark

J. Fluid Mech. (2017), *vol.* 831, *pp.* 289–329. © Cambridge University Press 2017
doi:10.1017/jfm.2017.626

Consistent equations for open-channel flows in the smooth turbulent regime with shearing effects

G. L. Richard[1,†], A. Rambaud[2] and J. P. Vila[3]

[1]Institut de Mathématiques de Toulouse; UMR5219, Université de Toulouse; CNRS; UPS IMT, F-31062 Toulouse CEDEX 9, France

[2]Universidad del Bío-Bío, depto de Matemática, Concepción, Chile

[3]Institut de Mathématiques de Toulouse; UMR5219, Université de Toulouse; CNRS; INSA, F-31077 Toulouse, France

(Received 24 March 2017; revised 20 July 2017; accepted 31 August 2017; first published online 13 October 2017)

Consistent equations for turbulent open-channel flows on a smooth bottom are derived using a turbulence model of mixing length and an asymptotic expansion in two layers. A shallow-water scaling is used in an upper – or external – layer and a viscous scaling is used in a thin viscous – or internal – layer close to the bottom wall. A matching procedure is used to connect both expansions in an overlap domain. Depth-averaged equations are then obtained in the approximation of weakly sheared flows which is rigorously justified. We show that the Saint-Venant equations with a negligible deviation from a flat velocity profile and with a friction law are a consistent set of equations at a certain level of approximation. The obtained friction law is of the Kármán–Prandtl type and successfully compared to relevant experiments of the literature. At a higher precision level, a consistent three-equation model is obtained with the mathematical structure of the Euler equations of compressible fluids with relaxation source terms. This new set of equations includes shearing effects and adds corrective terms to the Saint-Venant model. At this level of approximation, energy and momentum resistances are clearly distinguished. Several applications of this new model that pertains to the hydraulics of open-channel flows are presented including the computation of backwater curves and the numerical resolution of the growing and breaking of roll waves.

Key words: hydraulics, shallow water flows, turbulent boundary layers

1. Introduction

The Saint-Venant equations for shallow-water flows (Barré de Saint-Venant 1871) are widely used in open-channel hydraulics to describe gradually varied flows. However, the rapidly varied flows such as hydraulic jumps or bores are usually treated as hydraulic singularities. The Saint-Venant equations – also called the nonlinear shallow-water equations – can be seen as depth-averaged equations. The deviation of

† Email address for correspondence: gael.loic.richard@orange.fr

https://doi.org/10.1017/jfm.2017.626 Published online by Cambridge University Press

the velocity profile from a flat profile is neglected and an empirical friction law is usually added. The open-channel flow resistance is an important problem in hydraulics (see Yen 2002). The most frequently used friction laws are the Chézy formula (1769), the Gauckler–Manning–Strickler formula, which was proposed independently with some variants by Gauckler (1868), Manning (1895) and Strickler (1923), and the Darcy–Weisbach formula, formulated by d'Aubuisson de Voisins (1840), Weisbach (1845) and Darcy (1854) (see Chow 1959). In this latter law, the friction factor – called the Darcy or Darcy–Weisbach coefficient – can be estimated for smooth pipes by the Blasius relation if the Reynolds number is between 700 and 25 000 and by the Prandtl–Von Kármán relation if the Reynolds number is greater than 25 000 (Chow 1959; Yen 2002). The latter is a particular case of the Colebrook–White relation which is also valid for rough pipes. The values of the Darcy coefficient for smooth channels are considered to be very close to those of smooth pipes so that the same relations can be approximately used. However, experimental measurements of Tracy & Lester (1961) and Brock (1966, 1967) showed a measurable deviation and they proposed an empirical relation specially designed for smooth channels.

Other phenomena can be described with the Saint-Venant equations with a suitable friction law. For instance, Savage & Hutter (1989) used a solid friction law in the Saint-Venant equations for granular flows. The friction law was later improved by Pouliquen (1999) and was used to predict non-steady and non-uniform granular flows (Pouliquen & Forterre 2002).

The Saint-Venant equations are a set of two equations. The first one is a mass balance equation that can be derived from the depth averaging of the continuity equation. Averaging over the fluid depth Newton's second law leads to the momentum balance equation, which is the second equation of the system. The work-energy theorem – or theorem of the kinetic energy – can be also averaged over the depth, leading to an energy equation. In the case of the Saint-Venant system of equations, this energy equation is fully compatible with the momentum equations in the sense that it can be derived from the depth-averaged mass and momentum equations. However the difference between the physical meaning of the dissipation term in the energy equation and that of the friction term in the momentum equation was highlighted by several authors (Chow 1959; Yen 1973). The energy dissipation term represents 'the energy dissipated directly through viscosity into heat and the apparent loss of energy into turbulence through the transport and decay of the eddies that cannot be recovered by the mean motion' (Yen 2002) and is related to the work of the forces internal to the flow whereas the friction term represents the external forces acting on the boundary of the flow. Whether open-channel flow resistance is due to friction effects or to energy dissipation effects is a discussed problem but in many cases both are practically equivalent. This is not always the case though, especially not for hydraulic jumps where the friction can be neglected in the momentum balance equation but where there is a strong energy dissipation.

Attempts to take into account a non-flat velocity profile often involve shape factors. These shape factors are also used to describe a non-uniform velocity distribution in the direction transverse to the main direction of the flow. This three-dimensional effect will not be considered in this paper where the problem is supposed to be purely two-dimensional. If shape factors are used, the momentum equation and the energy equation lead to slightly different results because the shape factor that appears in the momentum flux – the Boussinesq coefficient – is slightly different from the shape factor of the energy flux – the Coriolis coefficient – (see Chow 1959, p. 40 and p. 51). This means also that the difference between energy and momentum resistances cannot be completely dismissed.

https://doi.org/10.1017/jfm.2017.626 Published online by Cambridge University Press

A different strategy to include deviation to a non-flat velocity profile was first introduced by Teshukov (2007) in the conservative case for three-dimensional shallow-water flows under the hypothesis of a weakly sheared flow. This approach involves a tensor depending on the deviation of the velocity components from their averaged values and includes an equation for this tensor. These equations are hyperbolic and admit a mathematical entropy but the tensor equations are not in a conservative form and dissipation is lacking. The case of two-dimensional flows was later studied by Richard & Gavrilyuk (2012) who derived a hyperbolic system of three equations in conservative form for mass, momentum and energy equations with empirical laws for friction and energy dissipation (Richard & Gavrilyuk 2013). The energy equation became an independent equation of the system and a third variable, called enstrophy, was added to the two variables of the Saint-Venant model. The resulting model has the mathematical structure of the compressible Euler equations with relaxation source terms. This approach provides an extension of the Saint-Venant equations and allows us to describe some rapidly varied flows with rollers such as hydraulic jumps and roll waves (Thual 2013).

It is therefore of great importance to describe correctly the dissipative effects in shallow-water flows and to include the energy balance equation in the models. The energy equation was used for viscous thin films in laminar flows to derive consistent two-equation models (Ruyer-Quil & Manneville 2000; Usha & Uma 2004; Luchini & Charru 2010*a*) and a three-equation model (Richard, Ruyer-Quil & Vila 2016) which has the structure of the Euler equations of compressible fluids with relaxation, diffusion and dispersion. Various modified Saint-Venant equations were proposed. The relevant flows in open-channel hydraulics are turbulent, with Reynolds numbers greater than 10^4. In spite of this, many models still rely on a laminar flow assumption. A turbulence model assuming a parabolic distribution of the eddy viscosity and a boundary condition with a friction law was proposed by Decoene *et al.* (2009). Luchini & Charru (2010*b*) used also a variable eddy viscosity satisfying a parabolic law and took into account the kinetic-energy balance equation. Their model is able to calculate the phase lead of the wall stress in a fully developed flow with important applications for the dynamics of an erodible bed.

We derive our equations from a turbulence model and from asymptotic expansions in two layers, an external layer and a viscous internal layer. The methods of matched asymptotic expansions were successfully used in fluid mechanics following the boundary layer theory of Prandtl (Van Dyke 1964). The relevant flows being turbulent with a very high Reynolds number, the viscous layer is very thin. In order for the method to work, the consistent expression of the velocity in the external layer can diverge towards the bottom but the depth-average value of this external velocity needs to be finite. A slightly different method, called method of successive complementary expansions, was implemented by Cousteix & Mauss (2004) to analyse high Reynolds number flows. This method allows us to obtain the theory of interactive boundary layer.

The main goal of this paper is to derive a consistent model for open-channel flows on a smooth bottom using a turbulence model and including an energy equation, keeping in mind the importance of having a simple mathematical structure to facilitate the numerical resolution. Another goal is to determine whether the classical Saint-Venant equations with a friction term and a negligible deviation from a flat velocity profile is a consistent set of equations at a certain level of approximation since this question is disputed. As it was underlined by Luchini & Charru (2010*b*), 'the widely used Saint-Venant – depth averaged – equations still rely on disputable

https://doi.org/10.1017/jfm.2017.626 Published online by Cambridge University Press

closure laws, for both the shape of the velocity profile and the bottom shear stress, of heuristic or empirical nature'. In § 2, we start from the Navier–Stokes equations with a mixing-length model of turbulence in the hypothesis of a smooth bottom. The mixing length is expressed with the Prandtl model modified by Van Driest's damping term. The shallow-water scaling is then presented followed by a viscous scaling appropriate in a thin viscous layer close to the bottom. An asymptotic expansion of the solution in both layers is presented in § 3 with a matching procedure to connect them in an overlap domain while preserving the consistency of balance momentum and energy over the thickness of the flow. Depth-averaged equations are derived in § 4. The approximation of weakly sheared flows is justified and the distinction between energy dissipation and friction is studied. Then the Saint-Venant equations with friction and a negligible deviation to a flat velocity profile are consistently recovered with a friction law which is compared to the Kármán–Prandtl law and to the measurements of Tracy & Lester (1961) and Brock (1966, 1967). A consistent three-equation model is then found at a higher level of precision. This model has the mathematical structure of the Euler equations of compressible fluids with relaxation source terms. It is the turbulent counterpart of the laminar model of Richard *et al.* (2016). Several applications of this model are presented in § 5 pertaining to the critical Froude number, the linear stability, the velocity of the kinematic waves, the total head and the shape factors. The backwater curves of the three-equation model are computed and compared to the classical ones. The numerical resolution of the equations is presented last and applied to the growing and breaking of roll waves.

2. Navier–Stokes equations with turbulence

2.1. *Navier–Stokes equations for two-dimensional flows down an incline*

We consider a two-dimensional thin liquid, flowing down an inclined plane. The angle of the plane with respect to the horizontal is θ. The directions Ox and Oz are respectively the directions parallel to the plane and normal to the plane. The components of the fluid velocity field are denoted by u and w in the directions Ox and Oz respectively. The bottom wall is smooth and the fluid depth is denoted by h (see figure 1).

The fluid motion is governed by the Navier–Stokes equations, completed by the boundary conditions on the bottom wall and at the free surface. The fluid is supposed to be incompressible and the capillarity is neglected. The continuity equation is

$$\frac{\partial u}{\partial x}+\frac{\partial w}{\partial z}=0. \tag{2.1}$$

The Navier–Stokes momentum equations in the Ox and Oz directions are:

$$\rho\left(\frac{\partial u}{\partial t}+\frac{\partial u^2}{\partial x}+\frac{\partial uw}{\partial z}\right)=\rho g\sin\theta-\frac{\partial p}{\partial x}+\frac{\partial \tau_{xx}}{\partial x}+\frac{\partial \tau_{xz}}{\partial z}, \tag{2.2}$$

$$\rho\left(\frac{\partial w}{\partial t}+\frac{\partial uw}{\partial x}+\frac{\partial w^2}{\partial z}\right)=-\rho g\cos\theta-\frac{\partial p}{\partial z}+\frac{\partial \tau_{xz}}{\partial x}+\frac{\partial \tau_{zz}}{\partial z}, \tag{2.3}$$

where g is the gravitational acceleration, p is the pressure and τ_{xx}, τ_{xz} and τ_{zz} are the components of the viscous stress tensor $\boldsymbol{\tau}$. The boundary conditions at the bottom are the no-penetration condition and the no-slip condition

$$w(z=0)=0, \quad u(z=0)=0. \tag{2.4a,b}$$

https://doi.org/10.1017/jfm.2017.626 Published online by Cambridge University Press

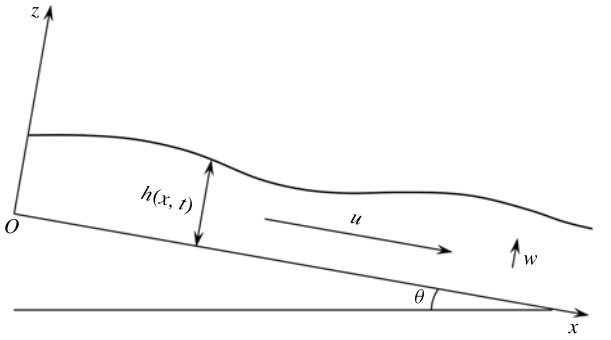


FIGURE 1. Notations used in the text.

At the free surface, the kinematic boundary condition holds

$$w(z=h)=\frac{\partial h}{\partial t}+u(z=h)\frac{\partial h}{\partial x}, \tag{2.5}$$

and the dynamic boundary condition

$$\left.\begin{aligned}[p(z=h)-\tau_{xx}(z=h)]\frac{\partial h}{\partial x}+\tau_{xz}(z=h)=0,\\ -\tau_{xz}(z=h)\frac{\partial h}{\partial x}-p(z=h)+\tau_{zz}(z=h)=0.\end{aligned}\right\} \tag{2.6}$$

The atmospheric pressure is constant and taken equal to zero.

2.2. *Mixing-length model: a nonlinear constitutive law of stress tensor*

The turbulence model of mixing length, initially proposed by Prandtl, is contained in the stress tensor. We denote by $\boldsymbol{D}$ the strain rate tensor. Instead of the classical viscous stress tensor for Newtonian fluids $\boldsymbol{\tau}=2\rho\nu\boldsymbol{D}$, where ν is the kinematic viscosity, we consider the constitutive law $\boldsymbol{\tau}=2\rho(\nu+\nu_T)\boldsymbol{D}$ where ν_T is the kinematic turbulent or eddy viscosity which depends on the z variable through a function L_m called the mixing length and on the norm of the tensor $\boldsymbol{D}$, namely:

$$\nu_T=\sqrt{2}\,L_m^2\|\boldsymbol{D}\|, \tag{2.7}$$

where the norm of the strain rate tensor is defined by

$$\|\boldsymbol{D}\|^2=2\left(\frac{\partial u}{\partial x}\right)^2+\frac{1}{2}\left(\frac{\partial u}{\partial z}+\frac{\partial w}{\partial x}\right)^2, \tag{2.8}$$

and the mixing length L_m depends on the chosen model. The first one is due to Prandtl:

$$L_m=\kappa z, \tag{2.9}$$

where κ is a dimensionless coefficient called the von Kármán constant. Its numerical value $\kappa\simeq 0.4$ is obtained from experimental data. This model was later modified by Van Driest (1951, 1956, 1959) who added a damping term

$$L_m=\kappa z(1-\mathrm{e}^{-z^+/A^+}), \tag{2.10}$$

https://doi.org/10.1017/jfm.2017.626 Published online by Cambridge University Press

where A^+ is also a dimensionless constant. The usual value is $A^+ = 26$. The dimensionless variable z^+ is often referred to as a viscous, or wall, coordinate. It is defined by $z^+ = zu_b/\nu$ where the shear velocity or friction velocity u_b is related to the bottom shear stress or parietal stress τ_b by $u_b = \sqrt{\tau_b/\rho}$ (see Henderson (1996), and equation (2.32) below). We define the (kinematic) effective viscosity as the sum of the molecular viscosity and the turbulent viscosity $\nu_{eff} = \nu + \nu_T$. The constitutive law can thus be written $\boldsymbol{\tau} = 2\rho\nu_{eff}\boldsymbol{D}$. To derive approximate one-dimensional (1-D) models, these equations are averaged over the depth. However we need two dimensionless systems in order to take into account the boundary layer near the bottom wall. Both scaling are presented next.

2.3. *Shallow-water scaling*

The equations are put into dimensionless form using a characteristic depth h_n as the characteristic length in the Oz direction and a characteristic speed in the Ox direction u_n. In practice, h_n and u_n are the depth and velocity of the uniform flow, called the normal depth and the normal velocity. The characteristic length in the Ox direction is L. The shallow-water hypothesis is that the aspect ratio ε is small:

$$\varepsilon = \frac{h_n}{L} \ll 1. \tag{2.11}$$

The dimensionless variables in this shallow-water scaling will be denoted with a prime. They are defined by

$$x' = \frac{x}{L}, \quad z' = \frac{z}{h_n}, \quad u' = \frac{u}{u_n}, \quad w' = \frac{w}{\varepsilon u_n}, \quad p' = \frac{p}{\rho g h_n}, \quad t' = \frac{t u_n}{L}. \tag{2.12a–f}$$

We define further $h' = h/h_n$, the Froude number $F = u_n/\sqrt{gh_n}$ and the Reynolds number $Re = h_n u_n/\nu$. We need a second Reynolds number related to the mixing length. The dimensionless mixing length L'_m can be defined by $L'_m = L_m/(\kappa h_n)$ and the dimensionless strain rate tensor by $\boldsymbol{D}' = h_n\boldsymbol{D}/u_n$. The components of $\boldsymbol{D}'$ can be written

$$\boldsymbol{D}' = \begin{bmatrix} \varepsilon\dfrac{\partial u'}{\partial x'} & \dfrac{1}{2}\left(\dfrac{\partial u'}{\partial z'} + \varepsilon^2\dfrac{\partial w'}{\partial x'}\right) \\ \dfrac{1}{2}\left(\dfrac{\partial u'}{\partial z'} + \varepsilon^2\dfrac{\partial w'}{\partial x'}\right) & \varepsilon\dfrac{\partial w'}{\partial z'} \end{bmatrix}, \tag{2.13}$$

so that:

$$\|\boldsymbol{D}'\| = \frac{1}{\sqrt{2}}\left|\frac{\partial u'}{\partial z'}\right| + O(\varepsilon^2). \tag{2.14}$$

The turbulent viscosity becomes $\nu_T = \kappa^2 h_n u_n \sqrt{2} L'^2_m \|\boldsymbol{D}'\|$. Taking $\nu_e = \kappa^2 h_n u_n$ as a characteristic eddy viscosity, we can define the dimensionless turbulent viscosity as $\nu'_T = \nu_T/\nu_e$. The mixing-length Reynolds number can be defined by

$$Re_{ML} = \frac{h_n u_n}{\nu_e} = \frac{1}{\kappa^2}. \tag{2.15}$$

Note that Re_{ML} is independent of the fluid depth. Its numerical value is close to 6. It is thus much smaller that the fluid Reynolds number which is supposed to be larger than

https://doi.org/10.1017/jfm.2017.626 Published online by Cambridge University Press

10^4. We obtain $\nu'_T = \sqrt{2} L'^2_m \|\boldsymbol{D}'\|$. The dimensionless viscous stress tensor is defined as $\boldsymbol{\tau}' = \boldsymbol{\tau}/(\rho\kappa^2 u_n^2)$. This gives $\boldsymbol{\tau}' = 2\,\nu'_{eff}\boldsymbol{D}'$ with $\nu'_{eff} = \nu'_T + \nu/\nu_e$. The ratio

$$\eta = \frac{Re_{ML}}{Re} = \frac{1}{\kappa^2 Re}, \tag{2.16}$$

is an important quantity. It can also be written $\eta = \nu/\nu_e$. Usual values of η lie in the range 10^{-4}–10^{-6}. A typical value of ε being 10^{-2}, we can assume that $\eta < \varepsilon$. In many cases, we have also $\eta < \varepsilon^2$ and this will be our choice. In the following, we will suppose that

$$\eta = \varepsilon^{2+m}, \quad m > 0. \tag{2.17}$$

The grounds for this choice are explained in § 3.2. The dimensionless effective viscosity can be written

$$\nu'_{eff} = \eta + \sqrt{2}\, L'^2_m \|\boldsymbol{D}'\|. \tag{2.18}$$

The expression of the dimensionless mixing length can be simplified as

$$L'_m = z' \left[1 - \exp\left(-\frac{z'\sqrt{\tau'_b}}{\eta\kappa A^+}\right)\right] \simeq z', \tag{2.19}$$

and the effective viscosity becomes

$$\nu'_{eff} = z'^2 \left|\frac{\partial u'}{\partial z'}\right| + O(\varepsilon^2). \tag{2.20}$$

With this scaling, the continuity equation (2.1) becomes simply

$$\frac{\partial u'}{\partial x'} + \frac{\partial w'}{\partial z'} = 0. \tag{2.21}$$

The momentum equation in the Oz direction (2.3) can be written

$$\frac{\partial p'}{\partial z'} = -\cos\theta + O(\varepsilon). \tag{2.22}$$

This means that the pressure is hydrostatic at this approximation. In this scaling, $\sin\theta$ is $O(1)$. Denoting

$$\lambda = \frac{\sin\theta}{\kappa^2 F^2}, \tag{2.23}$$

the momentum equation in the Ox direction (2.2) becomes

$$\frac{\varepsilon}{\kappa^2}\left(\frac{\partial u'}{\partial t'} + \frac{\partial u'^2}{\partial x'} + \frac{\partial u'w'}{\partial z'}\right) = \lambda + \frac{\partial \tau'_{xz}}{\partial z'} - \frac{\varepsilon}{\kappa^2 F^2}\frac{\partial p'}{\partial x'} + O(\varepsilon^2). \tag{2.24}$$

Another assumption for this model is that $\varepsilon/(\kappa^2 F^2) = O(\varepsilon)$. This implies that $F = O(1)$. The no-penetration and no-slip conditions are simply $w'(0) = 0$ and $u'(0) = 0$. Likewise the kinematic boundary condition at the free surface is the same as (2.5) but with dimensionless quantities (with a prime symbol). The dynamic boundary conditions at the free surface can be written

$$p'(h) = O(\varepsilon), \tag{2.25}$$

https://doi.org/10.1017/jfm.2017.626 Published online by Cambridge University Press

$$\tau'_{xz}(h) = O(\varepsilon^2). \tag{2.26}$$

However, the above scaling is not sufficient to provide a consistent description of the flow. In particular, this scaling leads to a singular expansion in the asymptotic regime we are interested in. Even at order zero, we cannot reach the Dirichlet boundary condition at the bottom. This lack of consistency with the physical boundary condition comes from the presence of the dimensionless parameter η which is very small in our asymptotic regime. Consequently, it is natural to introduce another scaling, called the viscous scaling, which is presented below.

2.4. *Viscous scaling*

This scaling is made in order to get suitable bounds of u, w, τ_{xz} and τ_{xx}, together with their time and spatial derivatives. Above all, this second scaling, only used near the bottom wall, allows us to recover consistency with boundary conditions (2.4). Actually, it consists in a zoom of the previous system close to the wall. This zoom is naturally done using the parameter η. We define dimensionless quantities in the viscous scaling, denoted with a tilde symbol. Some are the same as in the first scaling,

$$\tilde{x} = x', \quad \tilde{t} = t', \quad \tilde{u} = u', \quad \tilde{p} = p', \quad \tilde{\boldsymbol{\tau}} = \boldsymbol{\tau}', \tag{2.27a–e}$$

while others are magnified,

$$\tilde{z} = \frac{z'}{\eta}, \quad \tilde{w} = \frac{w'}{\eta}, \quad \tilde{h} = \frac{h'}{\eta}. \tag{2.28a–c}$$

We thus obtain the following viscous dimensionless mass and momentum balances:

$$\frac{\partial \tilde{u}}{\partial \tilde{x}} + \frac{\partial \tilde{w}}{\partial \tilde{z}} = 0, \tag{2.29}$$

$$\frac{\partial \tilde{\tau}_{xz}}{\partial \tilde{z}} = O(\eta), \tag{2.30}$$

$$\frac{\partial \tilde{p}}{\partial \tilde{z}} = O(\eta), \tag{2.31}$$

together with the boundary conditions $\tilde{w}(0) = 0$, $\tilde{u}(0) = 0$, $\tilde{w}(h) = \partial \tilde{h}/\partial \tilde{t} + \tilde{u}(h)\partial \tilde{h}/\partial \tilde{x}$, $\tilde{p}(h) = O(\varepsilon)$ and $\tilde{\tau}_{xz}(h) = O(\varepsilon^2)$. Note that our new variables are related to the classical viscous variables (see for example Henderson 1996; Sturm 2010):

$$\tilde{z} = z^+ \frac{\kappa^2 u_n}{u_b}, \quad \tilde{u} = u^+ \frac{u_n}{u_b}, \quad \tilde{h} = h^+ \frac{\kappa^2 u_n}{u_b}. \tag{2.32a–c}$$

Moreover, in this scaling, the dimensionless mixing length is magnified as $\tilde{L}_m = L'_m/\eta$, so that

$$\tilde{L}_m = \tilde{z}\left[1 - \exp\left(-\frac{\tilde{z}\sqrt{\tilde{\tau}_b}}{\kappa A^+}\right)\right], \tag{2.33}$$

while the strain rate tensor is $\tilde{\boldsymbol{D}} = \eta \boldsymbol{D}'$. The effective viscosity becomes

$$\tilde{\nu}_{eff} = 1 + \sqrt{2}\tilde{L}_m^2 \|\tilde{\boldsymbol{D}}\|, \tag{2.34}$$

with

$$\|\tilde{\boldsymbol{D}}\| = \frac{1}{\sqrt{2}}\left|\frac{\partial \tilde{u}}{\partial \tilde{z}}\right| + O(\varepsilon^2\eta). \tag{2.35}$$

https://doi.org/10.1017/jfm.2017.626 Published online by Cambridge University Press

3. Asymptotic expansions

3.1. General methodology

The asymptotic expansions of the solution to the dimensionless Navier–Stokes equations are built with an iterative algorithm, consisting in resolving a differential system at each order with respect to the small parameter ε. This method is formally the same as the method proposed in Noble & Vila (2013) for power-law laminar flows and in Richard *et al.* (2016) for laminar Newtonian flows. It is a little bit more tedious in the present case because of the singularity of the expansions. The formal Hilbert expansions of the solutions

$$u' = u'_0 + \varepsilon\, u'_1 + O(\varepsilon^2), \tag{3.1}$$

$$w' = w'_0 + \varepsilon\, w'_1 + O(\varepsilon^2), \tag{3.2}$$

$$p' = p'_0 + \varepsilon\, p'_1 + O(\varepsilon^2), \tag{3.3}$$

$$\tau'_{xz} = \tau'_0 + \varepsilon\, \tau'_1 + O(\varepsilon^2), \tag{3.4}$$

are put into the dimensionless Navier–Stokes equations in the shallow-water scaling. Since the resolution of this system at a given order gives some expressions that diverge when $z \to 0$, the same kind of expansions and computations will be done for the viscous system. For instance, the asymptotic expansion of $\tilde{u}$ will be $\tilde{u} = \tilde{u}_0 + \varepsilon\tilde{u}_1 + O(\varepsilon^2)$. The expressions obtained for the viscous system are valid in an internal layer (close to the bottom), whereas those obtained for the shallow-water scaling are valid in the external layer (above the internal layer). For $Re \gg 1$, or equivalently $\eta \ll 1$, the internal layer is very thin, hence the zoom $\tilde{z} = z'/\eta$. We assume the existence of a buffer layer or overlap domain at a depth $z/h = O(\sqrt{\eta})$. To get a consistent expansion, a matching procedure is used (see Cousteix & Mauss 2007, for example): both expressions must fit in the overlap domain defined by $\sqrt{\eta}\, b_1 h < z < \sqrt{\eta}\, b_2 h$ where b_1 and b_2 are two positive dimensionless numbers of $O(1)$. The assumption of such an overlap layer leads to a consistent model of order 1 with the proviso that (2.17) is satisfied (see § 3.2 and (3.15) below).

The different stages of the computations at each order are the following: first, τ_{xz} is obtained by the vertical integration of the momentum equation in the Ox direction; then $\partial u/\partial z$ is built thanks to the constitutive law; we can then reconstruct u by integration; the mass equation allows us to calculate the vertical velocity w; finally, the pressure p is obtained by the vertical integration of the momentum equation in the Oz direction. Once the algorithm is done at order k, we repeat the procedure at order $k+1$. In practice, the computations will be done only at order zero and order 1 (the computation at order 2 would add the computation of $\tau_{xx} = -\tau_{zz}$).

3.2. Order zero

At order zero, equation (2.24) reduces to $\partial\tau'_0/\partial z' = -\lambda$. Since $\tau'_{xz}(h) = O(\varepsilon^2)$ (equation (2.26)), the integration leads to

$$\tau'_0 = \lambda(h' - z'). \tag{3.5}$$

The constitutive law and the expression of the effective viscosity (2.20) give

$$\tau'_0 = z'^2 \left(\frac{\partial u'_0}{\partial z'}\right)^2. \tag{3.6}$$

https://doi.org/10.1017/jfm.2017.626 Published online by Cambridge University Press

Defining $s = z'/h'$, the inversion of this relation leads to

$$\frac{\partial u_0'}{\partial z'} = \sqrt{\frac{\lambda}{h'}} \frac{\sqrt{1-s}}{s}. \tag{3.7}$$

The velocity u_0' is obtained by integration

$$u_0' = u_0'(h') + \sqrt{\lambda h}[2\sqrt{1-s} + j(s)], \tag{3.8}$$

where the function j is defined by

$$j(s) = \ln s - 2\ln(1+\sqrt{1-s}) \tag{3.9}$$

and where $u_0'(h')$ is the velocity at the free surface ($s = 1$). The examination of the expressions of τ_0 and u_0' shows that, when $z' \to 0$, $\tau_0 \to \lambda h'$ whereas u_0' diverges. The matching procedure is needed to find the complete expression of u_0' (in particular the value of $u_0'(h')$).

In the viscous layer, equation (2.30) implies that $\tilde{\tau}_0$ is constant. The matching procedure for τ_0' is then straightforward:

$$\tau_0'(0) = \tilde{\tau}_0(0) = \tau_b' = \tilde{\tau}_b = \lambda h'. \tag{3.10}$$

The constitutive law, together with the expression (2.34) of the effective viscosity gives

$$\tilde{\tau}_0 = \frac{\partial \tilde{u}_0}{\partial \tilde{z}} + \tilde{z}^2[1 - \mathrm{e}^{-\tilde{z}\sqrt{\lambda h'}/(\kappa A^+)}]^2 \left(\frac{\partial \tilde{u}_0}{\partial \tilde{z}}\right)^2. \tag{3.11}$$

This equation is inverted by solving a second-order algebraic equation. It yields

$$\frac{\partial \tilde{u}_0}{\partial \tilde{z}} = \frac{2\lambda h'}{1 + \sqrt{1 + \xi^2[1 - \exp(-\xi/A)]^2}}, \tag{3.12}$$

where $\xi = 2\sqrt{\lambda h'}\tilde{z}$ and $A = 2\kappa A^+$. By integration, with the no-slip condition $\tilde{u}_0(0) = 0$, we find

$$\tilde{u}_0 = \sqrt{\lambda h'}\left[-\frac{\xi}{1+\sqrt{1+\xi^2}} + \ln(\xi + \sqrt{1+\xi^2}) + \mathcal{R}(\xi)\right], \tag{3.13}$$

where the function $\mathcal{R}$ is defined by

$$\mathcal{R}(\xi) = \int_0^\xi \frac{\mathrm{d}Z}{1 + \sqrt{1 + Z^2(1 - \mathrm{e}^{-Z/A})^2}} - \int_0^\xi \frac{\mathrm{d}Z}{1+\sqrt{1+Z^2}}. \tag{3.14}$$

This function has a finite limit when $\xi \to \infty$ which will be denoted by R. The expression (3.8) in the external layer and the expression (3.13) in the internal layer are now fitted by the matching procedure: we solve $u_0'(z = \sqrt{\eta}\, bh) = \tilde{u}_0(z = \sqrt{\eta}\, bh) + O(\sqrt{\eta})$, with $0 < b_1 < b < b_2$. It is possible provided that

$$u_0'(h') = \sqrt{\lambda h'}(R - 3 + 3\ln 2 + \ln M - \ln \eta) + O(\sqrt{\eta}), \tag{3.15}$$

https://doi.org/10.1017/jfm.2017.626 Published online by Cambridge University Press

where the function M is given by $M = 2\sqrt{\lambda h'^3}$. The term $O(\sqrt{\eta})$ has to be asymptotically smaller than ε in order to get consistency at order 1, hence the choice (2.17). There appears a term of $O(-\ln\eta)$. Let

$$\mu = -\frac{2}{\ln\eta}. \tag{3.16}$$

Thereafter, this parameter will be treated as a small parameter satisfying the condition:

$$\varepsilon < \mu < 1. \tag{3.17}$$

The significance of this point will be highlighted later in this paper (see § 4.3). By definition, the small parameter μ depends on ε as

$$\mu = -\frac{2}{2+m}\frac{1}{\ln\varepsilon}, \tag{3.18}$$

where m is defined in (2.17). Since

$$\forall p > 0, \quad \lim_{\varepsilon\to 0}(\varepsilon \ln^p \varepsilon) = 0, \tag{3.19}$$

the main small parameter ε is smaller than μ^p for any positive integer p if ε is small enough. Each term of the asymptotic expansions of a given order, such as u_1', is further expanded in a power series of this second small parameter μ.

The expression (3.15) shows that $u_0'(h')$ is of $O(\sqrt{\lambda}/\mu)$. As we want u_0' to be of $O(1)$, this implies that $\lambda = O(\mu^2)$. We thus assume

$$\lambda = \mu^2\lambda_0, \tag{3.20}$$

where $\lambda_0 = O(1)$. Then $M = 2\mu\sqrt{\lambda_0 h'^3}$, and the free surface velocity (3.15) becomes

$$u_0'(h) = \sqrt{\lambda_0 h'}[2 + \mu(R - 3 + 3\ln 2 + \ln M)] + O(\sqrt{\eta}). \tag{3.21}$$

Note that practically $\ln\mu = O(1)$. For instance, if $\eta \sim 10^{-4}$, $\ln\mu \sim -1.5$. Hence $\ln M = O(1)$. The complete expression of u_0' is finally

$$\frac{u_0'}{\sqrt{\lambda_0 h'}} = 2 + \mu[R - 3 + 3\ln 2 + \ln M + 2\sqrt{1-s} + j(s)]. \tag{3.22}$$

Even if neither u_0' nor $\tilde{u}_0$ are valid approximations of the velocity on the whole fluid depth, we can use any of them to compute an average velocity since they are integrable functions on $[0, h]$ and that the values of these integrals match up to a small error with respect to ε. The average value over the fluid depth of any quantity X being defined by

$$\langle X\rangle = \frac{1}{h}\int_0^h X\,\mathrm{d}z, \tag{3.23}$$

it is natural to compute the average velocity from the expression (3.22). Writing $U = \langle u\rangle$, this gives

$$\frac{U_0'}{\sqrt{\lambda_0 h'}} = 2 + \mu\left(R - \frac{11}{3} + 3\ln 2 + \ln M\right). \tag{3.24}$$

https://doi.org/10.1017/jfm.2017.626 Published online by Cambridge University Press

The vertical velocity is computed from the continuity equation. Taking into account the kinematic boundary condition at the free surface, the integration of (2.21) leads to

$$w'(z') = \frac{\partial h'}{\partial t'} - \frac{\partial}{\partial x'} \int_{h'}^{z'} u' \, \mathrm{d}z'. \tag{3.25}$$

To estimate the derivative of h' with respect to t', the continuity equation is averaged over the depth. Thanks to the no-penetration boundary condition, we get

$$\frac{\partial h'}{\partial t'} + \frac{\partial h' U'}{\partial x'} = 0. \tag{3.26}$$

Consequently, $\partial h'/\partial t'$ can be estimated by

$$\frac{\partial h'}{\partial t'} = -\frac{\partial h' U'_0}{\partial x'} + O(\varepsilon), \tag{3.27}$$

where U'_0 is given by (3.24). At order zero, the vertical velocity is found by

$$w'_0(z') = -\frac{\partial h' U'_0}{\partial x'} + \frac{\partial}{\partial x'} \left[h' \int_s^1 u'_0 \, \mathrm{d}s \right], \tag{3.28}$$

where $s = z'/h'$. The result of the calculation is

$$\frac{w'_0(s)}{\sqrt{\lambda_0 h'} \partial h'/\partial x'} = -s + \mu \left[1 - \sqrt{1-s} - \frac{s}{2}(R + 3\ln 2 + j(s) + \ln M) \right]. \tag{3.29}$$

Finally, the zeroth-order pressure is computed readily from (2.22):

$$p'_0 = (h' - z') \cos\theta. \tag{3.30}$$

Equation (2.31) implies that $\tilde{p}_0$ is constant in the internal layer. Connecting this constant by the usual matching procedure gives simply $\tilde{p}_0 = h' \cos\theta$.

3.3. *Order 1*

At order 1, the momentum equation in the Ox direction (2.24) is

$$\frac{\partial u'_0}{\partial t'} + \frac{\partial u'^2_0}{\partial x'} + \frac{\partial u'_0 w'_0}{\partial z'} = \kappa^2 \frac{\partial \tau'_1}{\partial z'} - \frac{1}{F^2} \frac{\partial p'_0}{\partial x'}. \tag{3.31}$$

Making use of the boundary condition at the free surface, integration of (3.31) gives:

$$\kappa^2 \tau'_1 = \frac{\partial}{\partial t'} \int_{h'}^{z'} u'_0 \, \mathrm{d}z' + \frac{\partial}{\partial x'} \int_{h'}^{z'} u'^2_0 \, \mathrm{d}z' + u'_0 w'_0 + \frac{1}{F^2} \frac{\partial}{\partial x'} \int_{h'}^{z'} p'_0 \, \mathrm{d}z'. \tag{3.32}$$

The valued of $\partial h'/\partial t$ is estimated with (3.27). A long calculation yields

$$\tau'_1 = \frac{\lambda_0 h'}{\kappa^2} \frac{\partial h'}{\partial x'} [T_0(s) + \mu T_1(s) + \mu^2 T_2(s)], \tag{3.33}$$

https://doi.org/10.1017/jfm.2017.626 Published online by Cambridge University Press

where $s = z'/h'$ and:

$$\left.\begin{aligned}
T_0(s) &= \left(1 - \frac{\cos\theta}{\lambda_0 F^2}\right)(1-s),\\
T_1(s) &= (R - 1 + 3\ln 2 + \ln M)(1-s) + \frac{\sqrt{1-s}}{3} + \frac{2}{3}s\sqrt{1-s} + \frac{1}{2}sj(s),\\
T_2(s) &= \left[\frac{R^2}{4} - \frac{R}{2} - \frac{2}{3} + \frac{3}{2}\left(R - 1 + \frac{3}{2}\ln 2\right)\ln 2\right.\\
&\quad \left. + \frac{1}{2}\left(R - 1 + 3\ln 2 + \frac{1}{2}\ln M\right)\ln M\right](1-s)\\
&\quad + \left(3 + \frac{R}{6} + \frac{\ln 2}{2} + \frac{1}{6}\ln M\right)\sqrt{1-s} + \frac{1}{3}(R + 3\ln 2 + \ln M)\, s\sqrt{1-s}\\
&\quad - 2\ln(1+\sqrt{1-s}) + \frac{5}{3}\sqrt{1-s}j(s) + \frac{1}{4}(2 + R + 3\ln 2 + \ln M)sj(s)\\
&\quad + \frac{1}{3}s\sqrt{1-s}j(s) + \frac{1}{2}sj(s)^2 - \frac{5}{3}\ln s.
\end{aligned}\right\} \tag{3.34}$$

It appears that τ_1' possesses a finite limit when $z' \to 0$ (or $s \to 0$), namely

$$\tau_1'(0) = \frac{\lambda_0 h'}{\kappa^2}\frac{\partial h'}{\partial x'}[T_0(0) + \mu T_1(0) + \mu^2 T_2(0)], \tag{3.35}$$

with

$$\left.\begin{aligned}
T_0(0) &= 1 - \frac{\cos\theta}{\lambda_0 F^2},\\
T_1(0) &= R - \tfrac{2}{3} + 3\ln 2 + \ln M,\\
T_2(0) &= \frac{7}{3} - \frac{19}{3}\ln 2 + \frac{9}{4}\ln^2 2 - \frac{R}{3} + \frac{3}{2}R\ln 2 + \frac{R^2}{4}\\
&\quad + \left(\frac{R}{2} - \frac{1}{3} + \frac{3}{2}\ln 2 + \frac{1}{4}\ln M\right)\ln M.
\end{aligned}\right\} \tag{3.36}$$

In the internal (viscous) layer, equation (2.30) implies that $\tilde{\tau}_1$ is constant. It follows from the matching procedure that this constant is equal to $\tau_1'(0)$ given by equation (3.35).

Next, the constitutive law and the external (shallow-water) effective viscosity (2.20) give

$$\tau_1' = 2z' \frac{\partial u_0'}{\partial z'}\frac{\partial u_1'}{\partial z'}. \tag{3.37}$$

The inversion of this relation gives

$$\frac{\partial u_1'}{\partial z'} = \frac{1}{2\kappa^2}\sqrt{\frac{\lambda_0}{h'}}\frac{\partial h'}{\partial x'}\frac{T_0(s) + \mu T_1(s) + \mu^2 T_2(s)}{\mu s\sqrt{1-s}}. \tag{3.38}$$

The expression of the velocity at order 1 in the external layer is found by integration:

$$u_1' = u_1'(h) + \frac{\sqrt{\lambda_0 h'}}{2\kappa^2}\frac{\partial h'}{\partial x'}\frac{1}{\mu}\int_1^s \frac{T_0(s) + \mu T_1(s) + \mu^2 T_2(s)}{s\sqrt{1-s}}\,\mathrm{d}s. \tag{3.39}$$

https://doi.org/10.1017/jfm.2017.626 Published online by Cambridge University Press

Because u_1' diverges when $s \to 0$, we proceed as for the zeroth order: the same calculation is done in the internal layer and both expressions are fitted in the overlap domain. With the constitutive law and the internal effective viscosity (2.34), we get

$$\tilde{\tau}_1 = \frac{\partial \tilde{u}_1}{\partial \tilde{z}} \left[1 + 2\tilde{z}^2 (1 - \mathrm{e}^{-\tilde{z}\mu\sqrt{\lambda_0 h'}/(\kappa A^+)})^2 \frac{\partial \tilde{u}_0}{\partial \tilde{z}} \right]. \tag{3.40}$$

Since $\tilde{\tau}_1$ is constant and equal to $\tau_1'(0)$,

$$\frac{\partial \tilde{u}_1}{\partial \tilde{z}} = \frac{\lambda_0 h'}{\kappa^2} \frac{\partial h'}{\partial x'} \frac{T_0(0) + \mu T_1(0) + \mu^2 T_2(0)}{\sqrt{1 + \xi^2 (1 - \mathrm{e}^{-\xi/A})^2}}, \tag{3.41}$$

where $\xi = 2\sqrt{\lambda h'}\tilde{z}$ and $A = 2\kappa A^+$. Integrating this expression from 0 to ξ, taking into account the no-slip condition, we find

$$\tilde{u}_1 = \frac{\sqrt{\lambda_0 h'}}{2\kappa^2} \frac{\partial h'}{\partial x'} \frac{1}{\mu} [T_0(0) + \mu T_1(0) + \mu^2 T_2(0)][\ln(\xi + \sqrt{1 + \xi^2}) + \mathcal{R}_1(\xi)], \tag{3.42}$$

where the function $\mathcal{R}_1$ is defined by

$$\mathcal{R}_1(\xi) = \int_0^\xi \left[\frac{1}{\sqrt{1 + Z^2 (1 - \mathrm{e}^{-Z/A})^2}} - \frac{1}{\sqrt{1 + Z^2}} \right] \mathrm{d}Z. \tag{3.43}$$

This function possesses a finite limit when $\xi \to \infty$ which will be denoted by R_1. The replacement of $\mathcal{R}_1(Mb/\sqrt{\eta})$ by R_1 in the matching procedure below is justified in a similar way as for R (see appendix A).

To match the external velocity with the inner one, we solve, for $0 < b_1 < b < b_2$,

$$u_1'(s = \sqrt{\eta} b) = \tilde{u}_1 \left(\xi = \frac{Mb}{\sqrt{\eta}} \right) + O(\sqrt{\eta}). \tag{3.44}$$

A very long calculation yields

$$u_1'(h) = \frac{\sqrt{\lambda_0 h'}}{\kappa^2} \frac{\partial h'}{\partial x'} \left[\frac{1}{\mu^2} \left(1 - \frac{\cos\theta}{\lambda_0 F^2} \right) + \frac{V_1}{\mu} + V_2 \right] + O(\mu), \tag{3.45}$$

where

$$\left.\begin{aligned} V_1 &= \frac{1}{2} \left[2R + R_1 - \frac{10}{3} + 9\ln 2 + 3\ln M + \frac{\cos\theta}{\lambda_0 F^2} (2 - R_1 - 3\ln 2 - \ln M) \right], \\ V_2 &= \frac{1}{2} \left[\frac{22}{3} - \frac{8}{3}R + \frac{R^2}{2} - \frac{2}{3}R_1 + RR_1 + \left(6R + 3R_1 - \frac{70}{3} + \frac{27}{2}\ln 2 \right) \ln 2 \right. \\ &\quad \left. + \left(2R + R_1 - \frac{10}{3} + 9\ln 2 + \frac{3}{2}\ln M \right) \ln M \right]. \end{aligned}\right\} \tag{3.46}$$

https://doi.org/10.1017/jfm.2017.626 Published online by Cambridge University Press

The final expression of u_1' is

$$u_1' = u_1'(h) + \frac{\sqrt{\lambda_0 h'}}{2\kappa^2}\frac{\partial h'}{\partial x'}\left[\left(1-\frac{\cos\theta}{\lambda_0 F^2}\right)\frac{2\sqrt{1-s}+j(s)}{\mu} + \frac{4}{3}\ln s + \frac{2}{3}(s-1)\right.$$
$$\left. + (R-1+3\ln 2+\ln M)(2\sqrt{1-s}+j(s)) - \sqrt{1-s}j(s)\right] + O(\mu). \qquad (3.47)$$

Even if this expression is not valid over the whole fluid depth (it diverges for $z \to 0$) and must be connected to the inner expression, u_1' possesses a finite average value over the whole depth. This first-order average velocity, denoted by $U_1' = \langle u_1' \rangle$ is given by:

$$U_1' = u_1'(h) - \frac{\sqrt{\lambda_0 h'}}{3\kappa^2}\frac{\partial h'}{\partial x'}\left[\frac{1}{\mu}\left(1-\frac{\cos\theta}{\lambda_0 F^2}\right) + R + \frac{1}{2} + \ln 2 + \ln M\right] + O(\mu). \qquad (3.48)$$

We are now able to derive our reduced models of smooth turbulent free surface flow.

4. Models

4.1. *Averaged equations*

Models are obtained from an averaging procedure over the fluid depth (see (3.23)) of the Navier–Stokes equations, taking into account the boundary conditions and the formal asymptotic expansions of § 3. An advantage of this approach is that the dimensionality of the model is one less than for the starting equations and that the boundary conditions are incorporated into the equations of the model. As a consequence, the numerical resolution is much faster and easier provided that the equations of the model have an appropriate mathematical structure.

The equations are averaged in the shallow-water scaling. We recall that we denote by $U' = \langle u' \rangle$ the average fluid velocity. The averaging of the continuity equation (2.21) was done above (equation (3.26)): note that it is exact. Next, let us average the momentum equation in the Ox-direction (2.24). At the first order of approximation, the pressure is hydrostatic (see (3.30)), so that we obtain

$$\frac{\partial h'U'}{\partial t'} + \frac{\partial}{\partial x'}\left[h'\langle u'^2\rangle + \frac{h'^2\cos\theta}{2F^2}\right] = \frac{\kappa^2}{\varepsilon}[\lambda h' - \tau_{xz}'(0)] + O(\varepsilon). \qquad (4.1)$$

The average quantity $\langle u'^2 \rangle$ is expressed by decomposing the velocity as the sum of its average value and a deviation u^* to this average value:

$$u' = U' + u^*. \qquad (4.2)$$

This method will be proved to be very similar to that used by Teshukov (2007). In particular, it will be shown below that the introduction of the small parameter μ in (3.16) is equivalent to Teshukov's approximation of weakly sheared flows (Teshukov 2007). Equation (4.1) becomes

$$\frac{\partial h'U'}{\partial t'} + \frac{\partial}{\partial x'}\left[h'U'^2 + h'\langle u^{*2}\rangle + \frac{h'^2\cos\theta}{2F^2}\right] = \frac{\kappa^2}{\varepsilon}[\lambda h' - \tau_{xz}'(0)] + O(\varepsilon). \qquad (4.3)$$

https://doi.org/10.1017/jfm.2017.626 Published online by Cambridge University Press

To handle $\langle u^{*2}\rangle$, a third variable called enstrophy is introduced as in Richard & Gavrilyuk (2012) and Richard *et al.* (2016). The enstrophy is defined as

$$\varphi' = \frac{\langle u^{*2}\rangle}{h'^2}. \tag{4.4}$$

One of the advantage of the enstrophy is that it acts as the mathematical entropy of the hyperbolic model (Richard & Gavrilyuk 2012). The momentum equation becomes

$$\frac{\partial h'U'}{\partial t'} + \frac{\partial}{\partial x'}\left[h'U'^2 + h'^3\varphi' + \frac{h'^2\cos\theta}{2F^2}\right] = \frac{\kappa^2}{\varepsilon}[\lambda h' - \tau'_{xz}(0)] + O(\varepsilon). \tag{4.5}$$

Since there are now three unknowns in the model, a third equation is needed to close the system. This equation is provided by the work-energy theorem also called theorem of the kinetic energy. In the present case, and in the shallow-water scaling, it reads

$$\begin{aligned}&\frac{\partial}{\partial t'}\left(\frac{u'^2}{2}\right) + \frac{\partial}{\partial x'}\left[u'\left(\frac{u'^2}{2} - \frac{x'\sin\theta}{\varepsilon F^2} + \frac{z'\cos\theta}{F^2}\right) + \frac{p'u'}{F^2}\right]\\ &\quad + \frac{\partial}{\partial z'}\left[w'\left(\frac{u'^2}{2} - \frac{x'\sin\theta}{\varepsilon F^2} + \frac{z'\cos\theta}{F^2}\right) + \frac{p'w'}{F^2} - \frac{\kappa^2}{\varepsilon}\tau'_{xz}u'\right]\\ &= -\frac{\kappa^2}{\varepsilon}\boldsymbol{\tau}' : \boldsymbol{D}' + O(\varepsilon),\end{aligned} \tag{4.6}$$

where the colon symbol denotes the double contraction. More explanations can be found in Richard *et al.* (2016). Averaging this equation over the depth, we get

$$\begin{aligned}&\frac{\partial}{\partial t'}\left[\frac{h'U'^2}{2} + \frac{h'^3\varphi'}{2} + \frac{h'^2\cos\theta}{2F^2}\right] + \frac{\partial}{\partial x'}\left[\frac{h'U'^3}{2} + \frac{3}{2}h'^3U'\varphi' + \frac{h'\langle u^{*3}\rangle}{2} + \frac{h'^2U'\cos\theta}{F^2}\right]\\ &\quad = \frac{\kappa^2}{\varepsilon}(\lambda h'U' - W') + O(\varepsilon),\end{aligned} \tag{4.7}$$

where W' is the dimensionless power dissipated inside the flow by effective viscous effects

$$W' = \int_0^{h'} \boldsymbol{\tau}' : \boldsymbol{D}'\,\mathrm{d}z'. \tag{4.8}$$

Up to now, we obtained a set of three equations: the mass equation (3.26), the momentum equation (4.5) and the energy equation (4.7). Note that $\langle u^{*3}\rangle$ appears in the latter. But we will see below that it is possible to get rid of it and thus to close the problem.

4.2. *Asymptotic expansion of the enstrophy and of* $\langle u^{*3}\rangle$

Since the enstrophy is a variable of the system, its asymptotic expansion is needed to build the model. We write $\varphi' = \varphi'_0 + \varepsilon\varphi'_1 + O(\varepsilon^2)$. Likewise, the velocity deviation is expanded as $u^* = u^*_0 + \varepsilon u^*_1 + O(\varepsilon^2)$ with $u^*_0 = u'_0 - U'_0$ and $u^*_1 = u'_1 - U'_1$. At order zero, the enstrophy is calculated by $\varphi'_0 = \langle u^{*2}_0\rangle/h'^2$:

$$\varphi'_0 = \mu^2\frac{\lambda_0}{h'}\frac{2}{9}(12\ln 2 - 5). \tag{4.9}$$

https://doi.org/10.1017/jfm.2017.626 Published online by Cambridge University Press

The expression of the enstrophy at order 1, computed from $\varphi_1' = 2\langle u_0^* u_1^* \rangle / h'^2$, is

$$\varphi_1' = \frac{\lambda_0}{\kappa^2 h'} \frac{\partial h'}{\partial x'} \left\{ \left(\frac{10}{9} - \frac{8}{3} \ln 2 \right) \left(\frac{\cos\theta}{\lambda_0 F^2} - 1 \right) + \mu \left[\frac{548}{135} - \frac{2}{9}\pi^2 - \frac{10}{9} R + \left(\frac{8}{3} R - \frac{62}{9} + 8 \ln 2 \right) \ln 2 + \left(\frac{8}{3} \ln 2 - \frac{10}{9} \right) \ln M \right] \right\} + O(\mu^2). \tag{4.10}$$

The asymptotic expansion at order zero of $\langle u^{*3} \rangle$ is

$$\langle u_0^{*3} \rangle = \mu^3 \sqrt{\lambda_0^3 h'^3} \left(\tfrac{172}{135} - \tfrac{2}{3}\pi^2 + \tfrac{16}{3} \ln 2 \right). \tag{4.11}$$

4.3. *Weakly sheared flows*

The asymptotic expansion at order zero of the velocity deviation is

$$u_0^* = \mu \sqrt{\lambda_0 h'} \left(\tfrac{2}{3} + 2\sqrt{1-s} + \ln s - 2 \ln(1 + \sqrt{1-s}) \right), \tag{4.12}$$

where $s = z'/h'$. This expression shows that $u_0^* = O(\mu)$. From the expression (4.9), we have $\varphi_0' = O(\mu^2)$ and from (4.11), $\langle u_0^{*3} \rangle = O(\mu^3)$. Consequently, these quantities are small since μ is a small parameter. The deviation of the velocity from its average value is small and this implies that the flow is weakly sheared. Teshukov formulated the approximation of weakly sheared flows by stating that the deviation of the velocity from its average value was of $O(\varepsilon^\beta)$ where $0 < \beta < 1$ (Teshukov 2007). Our approach allows us to recover Teshukov's approximation with μ replacing ε^β. Recall that μ is defined by (3.16), and satisfies (3.17). The condition $0 < \beta < 1$ is equivalent to $\varepsilon < \mu < 1$. For typical values of the Reynolds number in turbulent open-channel flows, i.e. $10^4 < Re < 10^7$, the parameter η lies in the range 6×10^{-7}–6×10^{-4}. We have then $0.14 < \mu < 0.27$ and also $2.0 \times 10^{-2} < \mu^2 < 7.3 \times 10^{-2}$ and $2.7 \times 10^{-3} < \mu^3 < 2.0 \times 10^{-2}$. The parameter μ is not independent of the small parameter ε (see (3.18)) and ε is smaller than μ^p for any positive integer p if ε is small enough (see (3.19)). In practice, ε has a small but finite value. The condition $\varepsilon < \mu < 1$ is satisfied for usual values of ε ($\sim 10^{-2}$) and Re. Further, the condition $\varepsilon < \mu^2$ can be acceptable. On the other hand, μ^3 is greater than ε only for very small values of ε and η (see in figure 2 the graphs of μ, μ^2 and μ^3 as functions of η). We can thus reasonably neglect terms of $O(\mu^3)$. Note that the asymptotic expansion is valid if $\varepsilon > \sqrt{\eta}$. More precisely $\eta = \varepsilon^{2+m}$, $m > 0$ (see (2.17)).

A similar approximation was used by Luchini & Charru (2010*b*) who introduced, after Mellor (1972), the small parameter u_b/U which is approximately proportional to $\ln^{-1}(Re_b)$ where $Re_b = hu_b/\nu$. The deviation of the velocity from its average value was taken into account by terms who were found to be of the order of $(u_b/U)^2$ while terms of the order of $(u_b/U)^3$ were neglected. The small parameter u_b/U plays the same role as our parameter μ which can be written $\mu = 2 \ln^{-1}(\kappa^2 Re)$.

Teshukov's approximation of weakly sheared flows allows us to neglect, in the energy equation, the term in $\langle u^{*3} \rangle$, which is of $O(\varepsilon^{3\beta})$ (see Teshukov (2007) for the general two-dimensional case or Richard & Gavrilyuk (2012) for the 1-D case). This is equivalent to neglect terms of $O(\mu^3)$ in our equations. Therefore we will neglect all terms of $O(\mu^3)$ and in particular, the term $\langle u^{*3} \rangle$. On the other hand, the terms with the enstrophy, which are of $O(\mu^2)$ in our approach or of $O(\varepsilon^{2\beta})$ in Teshukov's

https://doi.org/10.1017/jfm.2017.626 Published online by Cambridge University Press

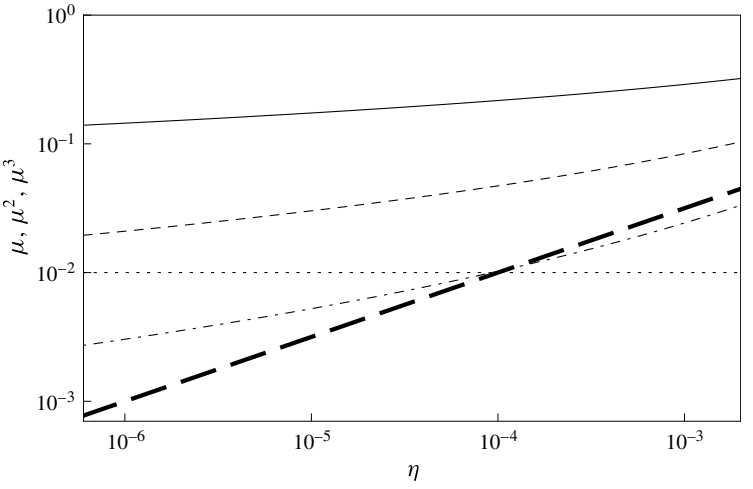


FIGURE 2. Values of μ (solid curve), μ^2 (dashed curve) and μ^3 (dot-dashed curve) as functions of η. The typical value $\varepsilon = 10^{-2}$ is shown (dotted line). The thick dashed curve is $\sqrt{\eta}$, which is the minimum value of ε for the model to be consistent.

approach, can be kept since, in practice, ε can be smaller than μ^2. The momentum equation (4.5) becomes

$$\frac{\partial h'U'}{\partial t'} + \frac{\partial}{\partial x'}[h'U'^2 + P'] = \frac{\kappa^2}{\varepsilon}[\lambda h' - \tau'_{xz}(0)] + O(\varepsilon), \tag{4.13}$$

and the energy equation (4.7)

$$\frac{\partial h'e'}{\partial t'} + \frac{\partial}{\partial x'}\left[h'U'\left(e' + \frac{P'}{h'}\right)\right] = \frac{\kappa^2}{\varepsilon}(\lambda h'U' - W') + O(\mu^3) + O(\varepsilon), \tag{4.14}$$

where

$$P' = h'^3\varphi' + \frac{h'^2\cos\theta}{2F^2}, \tag{4.15}$$

$$e' = \frac{1}{2}\left(U'^2 + h'^2\varphi' + \frac{h'\cos\theta}{F^2}\right). \tag{4.16}$$

Note that the left-hand side of system (4.13)–(4.14), together with (3.26), is analogous to the compressible Euler equations, with P' the pressure and e' the energy, the term $h'^2\varphi'/2 + h'\cos\theta/(2F^2)$ being the analogous of the internal energy (see Teshukov (2007) and Richard & Gavrilyuk (2012) for more explanations on this analogy).

4.4. *Asymptotic expansion of the dissipation power W*

The dissipation power W' is expanded as $W' = W'_0 + \varepsilon W'_1 + O(\varepsilon^2)$. Contrary to the integral of the velocity, the integral from 0 to h' of $\boldsymbol{\tau}' : \boldsymbol{D}'$, as expressed with the external expansion, diverges. To calculate W at any order, this integral should be divided into two parts, from the bottom to the overlap domain with the internal expansion and from the overlap domain to the free surface with the external expansion. The result depends on the exact position of the junction between the two parts.

https://doi.org/10.1017/jfm.2017.626 Published online by Cambridge University Press

Consequently, the direct calculation of this integral is not possible. Because there is not a single regular expansion from the bottom to the free surface, the first-order correction of the dissipation power W is not equal to zero and has to be calculated. Fortunately, the integral of the other terms of the energy equation, with the external expansion, does not diverge and can be used to calculate the dissipation power. At order zero, we get $W_0' = \lambda h' U_0'$, or

$$W_0' = \mu^2 (\lambda_0 h')^{3/2} \left[2 + \mu \left(R + 3 \ln 2 - \tfrac{11}{3} + \ln M \right) \right]. \tag{4.17}$$

The expression of W_1' is found with

$$\begin{aligned} W_1' = \mu^2 \lambda_0 h' U_1' - \frac{1}{\kappa^2} \frac{\partial}{\partial t'} \left(\frac{h' U_0'^2}{2} + \frac{h' \varphi'_0}{2} + \frac{h'^2 \cos\theta}{2F^2} \right) \\ - \frac{1}{\kappa^2} \frac{\partial}{\partial x'} \left(\frac{h' U_0'^3}{2} + \frac{3}{2} h'^3 U'_0 \varphi'_0 + \frac{h'^2 U'_0 \cos\theta}{F^2} \right). \end{aligned} \tag{4.18}$$

The result of this calculation is

$$W_1' = \frac{(\lambda_0 h')^{3/2}}{\kappa^2} \frac{\partial h'}{\partial x'} \left[3 \left(1 - \frac{\cos\theta}{\lambda_0 F^2} \right) + \mu Q_1 + \mu^2 Q_2 \right] + O(\mu^3), \tag{4.19}$$

where

$$\left.\begin{aligned} Q_1 &= -7 + 4R + \frac{R_1}{2} + \frac{27}{2} \ln 2 + \frac{\cos\theta}{\lambda_0 F^2} \left(5 - R - \frac{R_1}{2} - \frac{9}{2} \ln 2 \right) \\ &\quad + \frac{3}{2} \left(3 - \frac{\cos\theta}{\lambda_0 F^2} \right) \ln M, \\ Q_2 &= \frac{67}{6} - \frac{20}{3} R + \frac{7}{4} R^2 - \frac{R_1}{3} + \frac{R R_1}{2} - 39 \ln 2 + 12 R \ln 2 + \frac{3}{2} R_1 \ln 2 \\ &\quad + \frac{81}{4} \ln^2 2 + \left(-7 + 4R + \frac{R_1}{2} + \frac{27}{2} \ln 2 + \frac{9}{4} \ln M \right) \ln M. \end{aligned}\right\} \tag{4.20}$$

It is important to note that, in the general case, $W' \neq \tau'(0) U'$. At the order zero in μ, we have $W_0' = \tau_0'(0) U_0'$, but at the order $O(\mu^2)$, we get instead

$$W' = \tau'_{xz}(0) U' + \varepsilon \mu^2 \frac{(\lambda_0 h')^{3/2}}{3\kappa^2} \frac{\partial h'}{\partial x'} \left(\frac{5}{3} - 4 \ln 2 \right) + O(\varepsilon \mu^3). \tag{4.21}$$

This means that, if the shearing cannot be neglected i.e. at the order $O(\mu^2)$, which is the order of magnitude of the enstrophy, then the energy dissipation power is not the power of the friction force which appears in the averaged momentum equation. The difference between the momentum equation and the energy equation was clearly explained by several authors (Chow 1959, p. 51; Yen 1973, 2002): the averaged momentum equation involves only the forces external to the flow (in the present case the friction on the bottom wall). On the other hand, the energy equation, derived from the work-energy theorem includes the power of both the external and internal forces. Because of the no-slip condition, the friction force at the bottom does not do work. The dissipation power thus encompasses only the power dissipated by the

https://doi.org/10.1017/jfm.2017.626 Published online by Cambridge University Press

viscous forces, which are internal to the flow. Consequently, the dissipation power in the averaged energy equation has no reason to be always equal to the product of the bottom friction force and of the averaged velocity. The equality is true in the particular case of a negligible shearing, i.e. when the velocity is almost constant over the depth. In the case of a uniform flow, $\partial h'/\partial x' = 0$ and $W' = \tau'_{xz}(0)U' + O(\varepsilon\mu^3)$. This is also approximately the case if the flow is very gradually varied, i.e. when $|\partial h'/\partial x'| \ll 1$. Then the energy equation would be redundant, since it can be deduced from the mass and momentum equations. But when the shearing is not negligible, the averaged energy equation becomes independent of the averaged momentum equation. A third variable is necessary to take into account the shearing effect, for example the enstrophy (4.4), and the averaged energy equation provides the third equation needed to close the problem.

4.5. *Saint-Venant model*

The Saint-Venant model (Barré de Saint-Venant 1871) is an approximation of order 1 with respect to ε and with respect to μ (the enstrophy is negligible and $W = \tau(0)U$). The model has only two variables, for example h and U, and the energy equation is redundant. Since $\tau'_0(0) = \lambda h'$, equation (4.13) can be written

$$\frac{\partial h'U'}{\partial t'} + \frac{\partial}{\partial x'}\left[h'U'^2 + \frac{h'^2\cos\theta}{2F^2}\right] = -\kappa^2\tau'_1(0) + O(\varepsilon) + O(\mu^2). \tag{4.22}$$

Defining

$$C(\mu) = 2 + \mu(R + 3\ln 2 - \tfrac{11}{3} + \ln M), \tag{4.23}$$

so that the average velocity at order zero can be written $U'_0 = C(\mu)\sqrt{\lambda_0 h'}$, the following relation is satisfied:

$$\tau'_1(0) = \frac{\mu^2}{C(\mu)^2}2U'_0U'_1 + O(\mu). \tag{4.24}$$

Since

$$2U'_0U'_1 = \frac{U'^2 - U'^2_0}{\varepsilon} + O(\varepsilon), \tag{4.25}$$

equation (4.22) becomes

$$\frac{\partial h'U'}{\partial t'} + \frac{\partial}{\partial x'}\left[h'U'^2 + \frac{h'^2\cos\theta}{2F^2}\right] = \frac{\kappa^2}{\varepsilon}\left(\mu^2\lambda_0 h' - \frac{\mu^2}{C(\mu)^2}U'^2\right) + O(\varepsilon). \tag{4.26}$$

Let us define the friction coefficient C_f as

$$C_f = \frac{\mu^2\kappa^2}{C(\mu)^2}. \tag{4.27}$$

It is related to the usual Darcy coefficient (or Darcy–Weisbach coefficient) f by

$$f = 8C_f. \tag{4.28}$$

We may also relate it to the Fanning friction factor (equal to $2C_f$), or to the Chézy friction factor $C_h = \sqrt{g/C_f}$. As friction is irreversible, it cannot be invariant by a time

https://doi.org/10.1017/jfm.2017.626 Published online by Cambridge University Press

reversal transformation. Hence U'^2 is rewritten $U'|U'|$, and the momentum equation finally reads

$$\frac{\partial h'U'}{\partial t'} + \frac{\partial}{\partial x'}\left[h'U'^2 + \frac{h'^2\cos\theta}{2F^2}\right] = \frac{\kappa^2}{\varepsilon}\left(\lambda h' - \frac{C_f}{\kappa^2}U'|U'|\right) + O(\varepsilon). \tag{4.29}$$

Reverting to dimensional form and dropping the $O(\varepsilon)$ term, we obtain the following Saint-Venant system with friction

$$\frac{\partial h}{\partial t} + \frac{\partial hU}{\partial x} = 0, \tag{4.30}$$

$$\frac{\partial hU}{\partial t} + \frac{\partial}{\partial x}\left(hU^2 + \frac{gh^2\cos\theta}{2}\right) = gh\sin\theta - C_f U|U|, \tag{4.31}$$

which is the classical Saint-Venant system with a friction coefficient that has to be estimated numerically.

4.6. *Friction factor formula*

From the relations (4.23), (4.27) and (4.28), we can write

$$\frac{2\kappa\sqrt{2}}{\sqrt{f}} = R + 3\ln 2 - \frac{11}{3} + \ln\frac{2\sqrt{\lambda h'^3}}{\eta}. \tag{4.32}$$

For a uniform flow at normal depth and velocity, $h' = 1$, $U' = 1$ and $\lambda = C_f/\kappa^2$. The relation (4.32) can be written, using the decimal logarithm (noted lg),

$$\frac{1}{\sqrt{f}} = \frac{\ln 10}{2\kappa\sqrt{2}}\,\lg(Re\sqrt{f}) + \frac{1}{2\kappa\sqrt{2}}\left(R + \frac{5}{2}\ln 2 - \frac{11}{3} + \ln\kappa\right). \tag{4.33}$$

In hydraulics, the Reynolds number is often defined with the hydraulic diameter, which in the present case is equal to $4h$. Denoting by $Re_H = 4h_n u_n/\nu$ this Reynolds number, the equation (4.33) becomes

$$\frac{1}{\sqrt{f}} = \frac{\ln 10}{2\kappa\sqrt{2}}\,\lg(Re_H\sqrt{f}) + \frac{1}{2\kappa\sqrt{2}}\left(R + \frac{1}{2}\ln 2 - \frac{11}{3} + \ln\kappa\right). \tag{4.34}$$

Recall that

$$R = \lim_{\xi\to\infty}\mathcal{R}(\xi), \tag{4.35}$$

where function $\mathcal{R}$ is given by (3.14). Common values of the von Kármán constant are $\kappa = 0.41$ and $\kappa = 0.40$, although smaller or larger values have been reported. Recently, Bailey *et al.* (2014) measured the value $\kappa = 0.40 \pm 0.02$ for a fully developed turbulent flow in a hydraulically smooth pipe. The usual value of Van Driest damping constant is $A^+ = 26$ but here too, smaller or larger values have been proposed. Van Driest (1956) fitted experimental results of Laufer for fully developed turbulent flow in a smooth pipe with $\kappa = 0.4$ and $A^+ = 26$ but he mentioned that, in order to fit Nikuradse's smooth wall data, it would be necessary that $A^+ = 27$ (Van Driest 1956). With $\kappa = 0.41$ and $A^+ = 26$, the numerical value of the integral (4.35) is $R = 2.67$, and the relation (4.34) can be numerically written $1/\sqrt{f} = 2.0\lg(Re_H\sqrt{f}) - 1.33$. If $\kappa = 0.40$ and $A^+ = 27$, we get $R = 2.70$, and relation (4.34) becomes $1/\sqrt{f} = 2.035\lg(Re_H\sqrt{f}) - 1.36$. This relation is very similar to the Kármán–Prandtl law for pipes flows with smooth surfaces (or the Colebrook–White relation restricted to smooth surfaces), which is $1/\sqrt{f} = 2\lg(Re_H\sqrt{f}) - 0.8$.

https://doi.org/10.1017/jfm.2017.626 Published online by Cambridge University Press

The case of open-channel flows with a smooth bottom was studied experimentally by Tracy & Lester (1961) and by Brock (1966, 1967). Tracy & Lester made their experiments in a rectangular flume 1.07 m wide, 46 cm deep and 24.4 m long. In all, they made 49 uniform flow tests, 24 with a subcritical flow and 25 with a supercritical flow. The depth of the flow varied from 3 cm to 15 cm and the Reynolds number Re_H varied from 3.5×10^4 to 7×10^5. Their experimental results are plotted in figure 3. They fitted their data with the law (Tracy & Lester 1961)

$$\frac{1}{\sqrt{f}} = 2.03 \lg(Re_H \sqrt{f}) - 1.30. \tag{4.36}$$

This law is also plotted in figure 3 along with the Kármán–Prandtl law for turbulent flows in smooth pipes and our relation (4.34) expressed with two particular sets of values for κ and A^+. Brock (1966) made also friction measurements in supercritical flow with a smooth flume 1.1 m wide and 39.6 m long. The depth varied from 1.95 cm to 6.1 cm and the Reynolds number varied from $Re_H = 8.83 \times 10^4$ to $Re_H = 2.40 \times 10^5$. Other measurements were conducted by Brock (1967) in a smooth rectangular channel 11.7 cm wide and 24–39 m long with a depth between 5.2 mm and 10.4 mm and a Reynolds number Re_H between 1.63×10^4 and 7.07×10^4 with supercritical flows. These data are plotted in figure 3. For the first set of data, Brock fitted his experimental results with the law $1/\sqrt{f} = 2.03 \lg(Re_H \sqrt{f}) - 1.40$ (Brock 1966), which is very close to the law of Tracy & Lester. For the second set of data, the measures were found to follow the law of Tracy & Lester quite well with an averaged deviation of only 2.2 % (Brock 1967).

The equation (4.34) with usual values of the constants is very close to the law of Tracy & Lester and fits better the experimental measurements than the law for smooth pipes. Given the uncertainty on the values of the von Kármán constant and of Van Driest damping constant, the relation (4.34) is in good agreement with the experiments. We will use thereafter the values

$$\kappa = 0.40, \quad A^+ = 27, \tag{4.37a,b}$$

which are classical and which give a very good fit. Consequently,

$$R = 2.70 \tag{4.38}$$

and the relation (4.34) takes the numerical form

$$\frac{1}{\sqrt{f}} = 2.035 \lg(Re_H \sqrt{f}) - 1.36. \tag{4.39}$$

The friction factor formula having been tested in the case of uniform flows, relation (4.32) can be used for non-uniform flows. In dimensional form, this relation becomes

$$f = \frac{8\kappa^2}{\left(R + 4\ln 2 - \dfrac{11}{3} + \ln\kappa + \ln \dfrac{\sqrt{gh^3 \sin\theta}}{\nu}\right)^2}. \tag{4.40}$$

With the numerical values (4.37), we get

$$f = \frac{1.28}{\left(0.887 + \ln \dfrac{\sqrt{gh^3 \sin\theta}}{\nu}\right)^2}. \tag{4.41}$$

The friction coefficient decreases if the fluid depth increases. Qualitatively, the same effect is obtained if the Darcy factor is calculated using the empirical

https://doi.org/10.1017/jfm.2017.626 Published online by Cambridge University Press

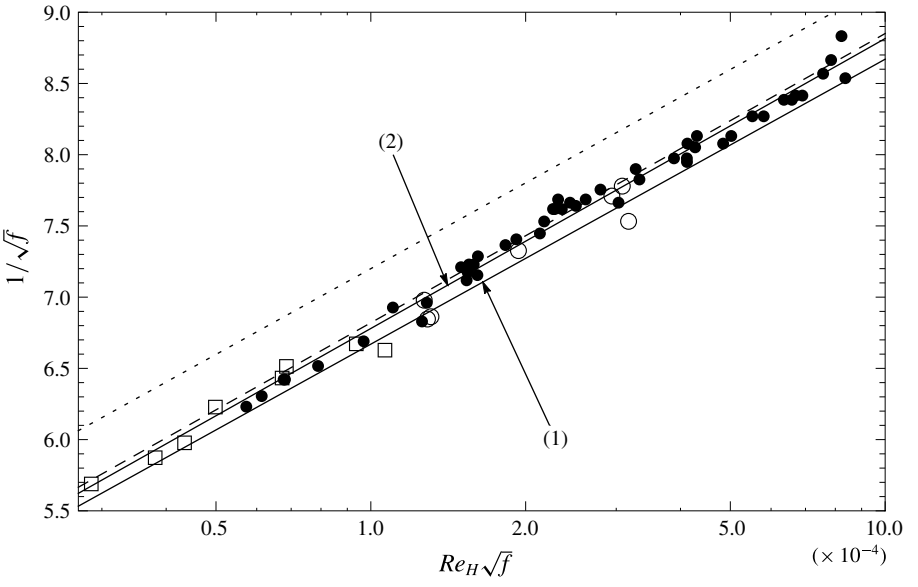


FIGURE 3. Variations of the Darcy friction factor. Experimental data: Tracy & Lester (1961): ●; Brock (1966): ○; Brock (1967): □. The solid line (1) is the relation (4.34) with $\kappa = 0.41$ and $A^+ = 26$. The solid line (2) is the same relation, with $\kappa = 0.40$ and $A^+ = 27$. The dashed line is the relation proposed by Tracy & Lester (1961) and the dotted line is the Kármán–Prandtl relation for smooth pipes.

Gauckler–Manning–Strickler formula: $f = 8g/(K_S^2 h^{1/3})$ where K_S is the Strickler coefficient. However the dependence with the depth is not the same although it is possible to find conditions where both relations are equivalent. A favourable case is presented in figure 4 with $\sin\theta = 10^{-4}$, $\nu = 10^{-6}$ m^2 s^{-1} and $K_S = 90$ m$^{1/3}$ s^{-1}. In other situations, the exponent 1/3 does not agree with relation (4.32). Note that the Gauckler–Manning–Strickler formula is valid for fully rough turbulent flows whereas relation (4.40) was derived in the case of a smooth turbulent regime. Thus we cannot expect a satisfactory agreement.

4.7. *Three-equation model*

At the order of $O(\mu^2)$, $W' \neq \tau'(0)U'$, and an additional variable is needed. Further, $\tau_1'(0) \neq \mu^2 2U_0'U_1'/C(\mu)^2$. Instead, we look for a relation of the form

$$\tau_1'(0) = \left(1 + A_1\frac{\kappa\mu}{C(\mu)} + A_2\frac{\kappa^2\mu^2}{C(\mu)^2}\right)\frac{\mu^2}{C(\mu)^2}2U_0'U_1' + \frac{\alpha'}{\kappa^2}\left(B_1\frac{\kappa\mu}{C(\mu)} + B_2\frac{\kappa^2\mu^2}{C(\mu)^2}\right)h'^2\varphi_1' + O(\mu^3), \tag{4.42}$$

where $C(\mu)$ is given by (4.23) and $\alpha' = 9\kappa^2/(2(12\ln 2 - 5))$. Similarly, we write

$$W_1' - \lambda h' U_1' = \left(1 + A'_1\frac{\kappa\mu}{C(\mu)} + A'_2\frac{\kappa^2\mu^2}{C(\mu)^2}\right)\frac{\mu^2}{C^2}2U_0'^2U_1' + \frac{\alpha'}{\kappa^2}\left(B'_1\frac{\kappa\mu}{C(\mu)} + B'_2\frac{\kappa^2\mu^2}{C(\mu)^2}\right)h'^2\varphi_1'U_0' + O(\mu^3). \tag{4.43}$$

https://doi.org/10.1017/jfm.2017.626 Published online by Cambridge University Press

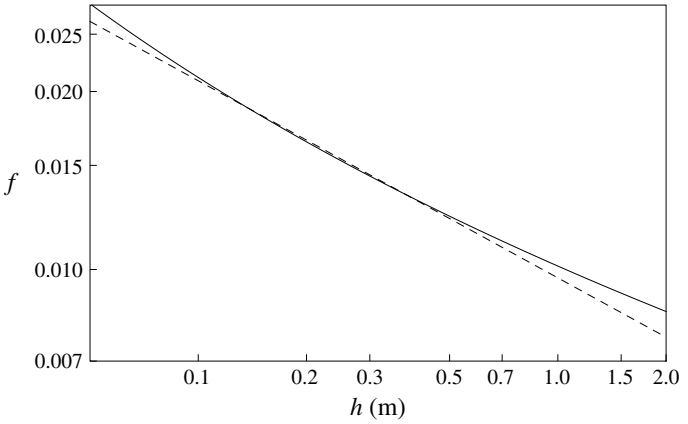


FIGURE 4. Variations of the Darcy friction factor with the fluid depth for $\sin\theta = 10^{-4}$ and with $\nu = 10^{-6}$ m^2 s^{-1} (solid curve) from relation (4.41). The dashed line is the Gauckler–Manning–Strickler formula with a Strickler coefficient $K_S = 90$ m$^{1/3}$ s^{-1}.

If solutions can be found for A_1, B_1, A_2, B_2, A_1', B_1', A_2' and B_2', the resulting model will be convenient since $C_f = \kappa^2\mu^2/C(\mu)^2$. The following numbers are introduced:

$$\left.\begin{aligned} &\alpha = (R_1 + 1 - R)/\kappa, \\ &\alpha_1 = \frac{45\pi^2\kappa\alpha + 672(R - R_1) - 797 + [960 + 360(R_1 - R) - 720\ln 2]\ln 2}{3\kappa(-224 + 15\pi^2 + 120\ln 2)}. \end{aligned}\right\} \quad (4.44)$$

With the values (4.37) of the von Kármán and Van Driest constants, the numerical values of α, α_1 and α' are

$$\alpha \simeq 7.93, \quad \alpha' \simeq 0.217, \quad \alpha_1 \simeq 1.58. \quad (4.45a\text{–}c)$$

Moreover, with the same values, the numerical value of R_1 defined as the limit of $\mathcal{R}_1(\xi)$ when $\xi \to \infty$ (see (3.43)), is $R_1 \simeq 4.87$.

Consistency is achieved at order $O(\mu)$ if $A_1 + B_1 = -\alpha$ and $A_1' + B_1' = -\alpha$. Consistency at order $O(\mu^2)$ implies $A_1 = -\alpha_1$, $B_1 = \alpha_1 - \alpha$, $A_1' = -\alpha$, $B_1' = 0$, $A_2 + B_2 = \alpha\alpha_1$ and $A_2' + B_2' = \alpha^2$. There is some freedom to choose the coefficients A_2, B_2, A_2' and B_2'.

However, it is interesting to see what happens if the Froude number is small. The assumption was that F was of $O(1)$. Since λ is of $O(\mu^2)$, this means that $\sin\theta$ is of $O(\mu^2)$. It is possible to assume that F is of $O(\mu)$ without changing the whole asymptotic expansion. In this case, $\sin\theta$ is of $O(\mu^4)$. The same asymptotic expansion can be used replacing only F by μF_0 with $F_0 = O(1)$. This changes only the order of some terms with respect to μ. Then the same procedure as above is repeated to find A_1, B_1, A_2, B_2, A_1', B_1', A_2' and B_2'. This time, there is only one solution. This solution gives exactly the same values as above for A_1, B_1, A_1' and B_1' and gives $A_2 = 0$; $B_2 = \alpha\alpha_1$; $A_2' = 0$; $B_2' = \alpha^2$. These values are a possible choice for the case above where $F = O(1)$. To get a complete compatibility between the model with $F = O(1)$ and the case of a low Froude number, these values of A_2, B_2, A_2' and B_2' were chosen. Note that this choice is also compatible with a high Froude number $F = F_0/\mu$, which corresponds to a high slope $\sin\theta = O(1)$.

https://doi.org/10.1017/jfm.2017.626 Published online by Cambridge University Press

With this choice, the relations (4.42) and (4.43) are rewritten respectively

$$\tau_1'(0) = \left(1 - \alpha_1 \frac{\kappa\mu}{C}\right) \frac{\mu^2}{C^2} 2U_0' U_1' - \frac{\alpha'}{\kappa} \left(\alpha - \alpha_1 - \alpha\alpha_1 \frac{\kappa\mu}{C}\right) \frac{\mu}{C} h'^2 \varphi_1' + O(\mu^3), \tag{4.46}$$

$$W_1 - \lambda h' U_1' = \left(1 - \kappa\alpha \frac{\mu}{C}\right) \frac{\mu^2}{C^2} 2U_0'^2 U_1' + \alpha^2 \alpha' \frac{\mu^2}{C^2} h'^2 \varphi_1' U_0' + O(\mu^3). \tag{4.47}$$

Since

$$2U_0' U_1' = \frac{U'^2 - U_0'^2}{\varepsilon} + O(\varepsilon), \quad \varphi_1' = \frac{\varphi' - \varphi_0'}{\varepsilon} + O(\varepsilon), \tag{4.48a,b}$$

and

$$2U_0'^2 U_1' = \frac{U'^2 - U_0'^2}{\varepsilon} U' + O(\varepsilon), \quad \varphi_1' U_0' = \frac{\varphi' - \varphi_0'}{\varepsilon} U' + O(\varepsilon), \tag{4.49a,b}$$

the average momentum equation (4.13) becomes, with the definition of C_f (4.27),

$$\begin{aligned} \frac{\partial h' U'}{\partial t'} + \frac{\partial}{\partial x'}[h' U'^2 + P'] = {} & \frac{\kappa^2}{\varepsilon}(1 - \alpha_1 \sqrt{C_f}) \left(\lambda h' - \frac{C_f}{\kappa^2} U' |U'|\right) \\ & + \frac{\kappa^2}{\varepsilon}(\alpha - \alpha_1 - \alpha\alpha_1 \sqrt{C_f}) \sqrt{C_f} \left(\frac{\alpha'}{\kappa^2} h'^2 \varphi' - \lambda h'\right) + O(\mu^3) + O(\varepsilon). \end{aligned} \tag{4.50}$$

The average energy equation (4.14) is then

$$\begin{aligned} \frac{\partial h' e'}{\partial t'} + \frac{\partial}{\partial x'} \left[h' U' \left(e' + \frac{P'}{h'}\right)\right] = {} & \frac{\kappa^2}{\varepsilon}(1 - \alpha \sqrt{C_f}) \left(\lambda h' - \frac{C_f}{\kappa^2} U' |U'|\right) U' \\ & - \frac{\kappa^2}{\varepsilon} \alpha^2 C_f \left(\frac{\alpha'}{\kappa^2} h'^2 \varphi' - \lambda h'\right) U' + O(\mu^3) + O(\varepsilon). \end{aligned} \tag{4.51}$$

From these equations, an equation for the enstrophy is derived:

$$\begin{aligned} \frac{\partial h' \varphi'}{\partial t'} + \frac{\partial h' U' \varphi'}{\partial x'} = {} & -\frac{\kappa^2}{\varepsilon} \frac{2(\alpha - \alpha_1)\sqrt{C_f}}{h'^2} U' \left[\lambda h' - \frac{C_f}{\kappa^2} U' |U'| \right. \\ & \left. + (1 + \alpha \sqrt{C_f}) \left(\frac{\alpha'}{\kappa^2} h'^2 \varphi' - \lambda h'\right)\right] + O(\mu^3) + O(\varepsilon). \end{aligned} \tag{4.52}$$

These equations (4.50)–(4.52) are consistent to the first order. The terms of order 0 appear only in relaxation terms that are written as differences between two order-zero quantities. The results of these differences are of first order as it is shown by equations (4.48)–(4.49).

Reverting to dimensions, the complete three-equation model reads:

$$\frac{\partial h}{\partial t} + \frac{\partial hU}{\partial x} = 0, \tag{4.53}$$

$$\begin{aligned} \frac{\partial hU}{\partial t} + \frac{\partial}{\partial x}[hU^2 + P] = {} & (1 - \alpha_1 \sqrt{C_f})(gh \sin\theta - C_f U |U|) \\ & + (\alpha - \alpha_1 - \alpha\alpha_1 \sqrt{C_f}) \sqrt{C_f} (\alpha' h^2 \varphi - gh \sin\theta), \end{aligned} \tag{4.54}$$

https://doi.org/10.1017/jfm.2017.626 Published online by Cambridge University Press

$$\frac{\partial he}{\partial t} + \frac{\partial}{\partial x}\left[hU\left(e + \frac{P}{h}\right)\right] = (1 - \alpha\sqrt{C_f})(gh\sin\theta - C_f U|U|)U - \alpha^2 C_f(\alpha' h^2\varphi - gh\sin\theta)U, \tag{4.55}$$

where

$$e = \tfrac{1}{2}(U^2 + h^2\varphi + gh\cos\theta), \tag{4.56}$$

$$P = h^3\varphi + \frac{gh^2\cos\theta}{2}. \tag{4.57}$$

The friction factor $C_f = f/8$ satisfies the consistent local law (4.40), and the numerical values of the constants α, α' and α_1 are given in (4.45). We may replace the last equation by the enstrophy equation:

$$\frac{\partial h\varphi}{\partial t} + \frac{\partial hU\varphi}{\partial x} = -2(\alpha - \alpha_1)\frac{\sqrt{C_f}}{h^2}U\big[gh\sin\theta - C_f U|U| + (1 + \alpha\sqrt{C_f})(\alpha' h^2\varphi - gh\sin\theta)\big]. \tag{4.58}$$

The equations of Saint-Venant are formally recovered by taking $\alpha = 0$, $\alpha_1 = 0$ and $\varphi = 0$. The present model adds corrective terms to the usual relaxation term for U and a new relaxation term for φ. The model features a new term in the energy, $h^2\varphi/2$, which is the additional kinetic energy due to shearing.

5. Applications

Some consequences of the new model (4.53)–(4.55) and comparison with the classical Saint-Venant system are examined here. We consider the system where the energy equation (4.55) is replaced by the enstrophy equation (4.58), except if discontinuities can arise.

5.1. *Characteristic velocities*

The left-hand side of system (4.53)–(4.55) is the same as in Richard & Gavrilyuk (2012). The right-hand side has only relaxation terms, so the model is hyperbolic, as it was proved by Teshukov (2007) and Richard & Gavrilyuk (2012). We rewrite the system in the matrix form

$$\frac{\partial \boldsymbol{V}}{\partial t} + \boldsymbol{A}\frac{\partial \boldsymbol{V}}{\partial x} = \boldsymbol{S}, \tag{5.1}$$

where $\boldsymbol{V} = [h, U, \varphi]^{\mathrm{T}}$, $\boldsymbol{S}$ is the matrix of the source terms (which plays no role in the following) and where the matrix $\boldsymbol{A}$ is

$$\boldsymbol{A} = \begin{bmatrix} U & h & 0 \\ g\cos\theta + 3h\varphi & U & h^2 \\ 0 & 0 & U \end{bmatrix}. \tag{5.2}$$

The three characteristic velocities of the model are the eigenvalues of this matrix. Their expressions are (Richard & Gavrilyuk 2012):

$$U, \quad U + \sqrt{gh\cos\theta + 3h^2\varphi}, \quad U - \sqrt{gh\cos\theta + 3h^2\varphi}. \tag{5.3a–c}$$

https://doi.org/10.1017/jfm.2017.626 Published online by Cambridge University Press

The two characteristic velocities of the model of Saint-Venant are $U+\sqrt{gh\cos\theta}$ and $U-\sqrt{gh\cos\theta}$. This means that taking into account shearing effects by the first-order correction modifies the expression of the speed of the surface waves. Consequently, the dimensionless number which represents the ratio of the fluid average velocity to the speed of the surface waves is not the classical Froude number

$$Fr=\frac{U}{\sqrt{gh\cos\theta}}, \tag{5.4}$$

but the number

$$Te=\frac{U}{\sqrt{gh\cos\theta+3h^2\varphi}}, \tag{5.5}$$

which depends not only of h and U but also on the enstrophy φ. As in Richard (2013), we propose to call this number the Teshukov number (Te) in honour of Vladimir Mikhailovich Teshukov (1946–2008), corresponding member of the Russian Academy of Sciences and director of the Lavrentiev Institute of Hydrodynamics (Novosibirsk), who first proposed this hyperbolic structure of equations for shallow-water flows and first derived the characteristic velocities in the general 2-D case (Teshukov 2007). A critical flow is thus defined by $Te=1$ instead of $Fr=1$. A subcritical flow and a supercritical flow are respectively defined by $Te<1$ and $Te>1$. For $Te>1$, no surface wave can propagate upstream.

Recalling our new friction formula (4.40), we obtain, by considering the equilibrium state as the uniform flow, with normal depth h_n and normal average velocity U_n, a normal friction factor, denoted C_n in the following, which reads

$$C_n=\kappa^2\left(R+4\ln 2-\frac{11}{3}+\ln\kappa+\ln\frac{\sqrt{gh_n^3\sin\theta}}{\nu}\right)^{-2}. \tag{5.6}$$

Given that $U_n=\sqrt{gh_n\sin\theta/C_n}$ and that the enstrophy of the steady uniform flow is $\varphi_n=g\sin\theta/(\alpha' h_n)$, the corresponding Teshukov and Froude numbers are, respectively:

$$Te_n=\sqrt{\frac{\mathrm{tg}\theta}{C_n}}\frac{1}{\sqrt{1+3\dfrac{\mathrm{tg}\theta}{\alpha'}}},\quad Fr_n=\sqrt{\frac{\mathrm{tg}\theta}{C_n}}=Te_n\sqrt{1+3\mathrm{tg}\theta/\alpha'}. \tag{5.7a,b}$$

The critical Froude number corresponds to $Te_n=1$ and is thus

$$Fr_0=\sqrt{1+\frac{3C_n}{\alpha'-3C_n}}. \tag{5.8}$$

It is higher than the classical value $Fr=1$ of the Saint-Venant equations. This result differs from Luchini & Charru (2010*b*) who found a critical Froude number smaller than 1. In practice, the critical Froude number is only slightly higher than 1 since $C_n\ll 1$. As C_n is determined if the Reynolds number is fixed, the critical Froude number depends only on the Reynolds number and on the value of α' which is taken as equal to 0.217 (see (4.45)). Figure 5 shows the variation of Fr_0 with the Reynolds number. The critical Froude number is never higher than 1.05 and is in the range 1.01–1.03 in most cases. It is doubtful whether such a small difference could be measured experimentally.

https://doi.org/10.1017/jfm.2017.626 Published online by Cambridge University Press

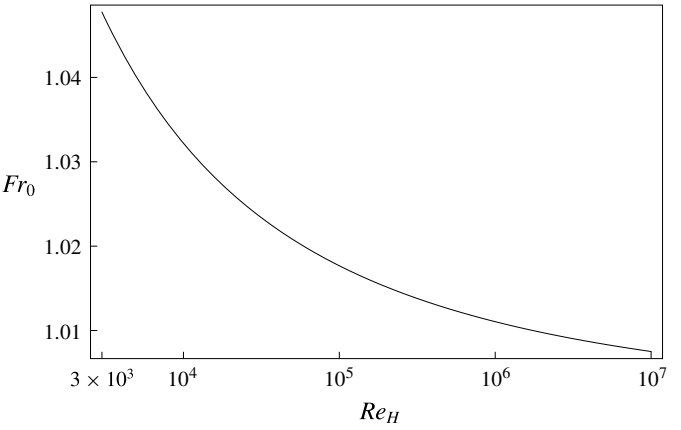


FIGURE 5. Critical Froude number governing the transition between a subcritical and a supercritical flow as a function of the Reynolds number for an equilibrium flow.

5.2. *Linear stability*

The characteristic velocities depend only on the conservative part of the equations and not on the relaxation terms. On the contrary, the linear stability and the expression of the velocity of the kinematic waves depend strongly on the relaxation source terms and thus on the friction factor. We linearize the system (4.53)–(4.55) around an equilibrium flow with a normal depth h_n, a normal velocity $U_n = \sqrt{gh_n \sin\theta / C_n}$ and a normal enstrophy $\varphi_n = g \sin\theta/(\alpha' h_n)$. The normal friction coefficient C_n is given by (5.6). We write $h = h_n + h'$, $U = U_n + U''$ and $\varphi = \varphi_n + \varphi''$, where h'', U'' and φ'' are small sinusoidal perturbations of h, U and φ, namely $[h'',\ U'',\ \varphi'']^{\mathrm{T}} = [A_1, A_2, A_3]^{\mathrm{T}} \exp[\mathrm{i}k(x - ct)]$.

The dispersion relation is found by writing that the determinant of this system is equal to zero to have a non-trivial solution. At the lowest order in the wavenumber k ($k \to 0$), the velocity c is the velocity of the kinematic waves denoted by c_0. In the case of the Saint-Venant model, with a constant friction factor, the velocity of the kinematic waves is $c_0/U_n = 3/2$. If the friction factor is supposed to follow the law of Gauckler–Manning–Strickler, the velocity of the kinematic waves is $c_0/U_n = 5/3$. In the present model, the friction factor is $C_f = f/8$, with f given by (4.40). Then $C_f(h_n + h'') = C_n + h'\,\partial C_f/\partial h(h = h_n)$. The velocity of the kinematic waves is given by

$$\frac{c_0}{U_n} = \frac{3}{2}\left(1 + \frac{\sqrt{C_n}}{\kappa}\right). \tag{5.9}$$

Since the normal friction factor C_n depends only on the Reynolds number Re, the velocity of the kinematic waves depends only on Re and on the value chosen for the constants, in particular the von Kármán constant. Taking the numerical values (4.37), the velocity c_0 is plotted as a function of Re in figure 6(*a*).

The velocity of the kinematic waves decreases if the Reynolds number increases and, as a whole, is not very different from the value given by the Gauckler–Manning–Strickler law. However, the value of c_0/U_n is significantly larger than the value of $3/2$ found if the friction factor is assumed to be a constant. This value of $3/2$ is the limit obtained if $Re \to \infty$ but the convergence is very slow and practically, c_0/U_n is always higher than 1.63, especially given that the assumption of a smooth turbulent regime

https://doi.org/10.1017/jfm.2017.626 Published online by Cambridge University Press

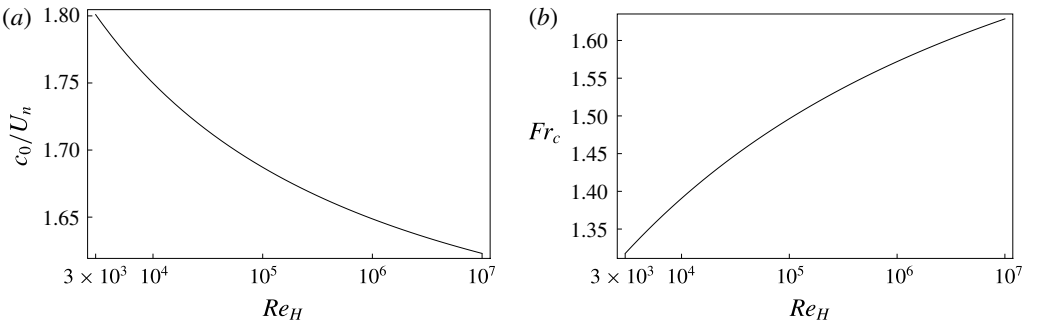


FIGURE 6. (*a*) Velocity of the kinematic waves as a function of the Reynolds number; (*b*) critical Froude number governing the instability of an equilibrium flow as a function of the Reynolds number.

becomes more and more restrictive when the Reynolds number increases. For not too high Reynolds numbers ($Re \sim 10^4$), c_0/U_n can be as high as 1.75 or more, thus larger than the value of the Gauckler–Manning–Strickler law.

The equilibrium flow becomes unstable if the Froude number is larger than a critical Froude number Fr_c, not to be confused with the critical Froude number Fr_0 of § 5.1. For the model of Saint-Venant, if the friction factor is supposed to be constant, this critical Froude number is $Fr_c = 2$. If the friction factor is supposed to follow the Gauckler–Manning–Strickler law, the critical Froude number is $Fr_c = 3/2$. In the case of the present model, the critical Froude number is

$$Fr_c = 2\sqrt{\frac{N_0 + N_1\sqrt{C_n}}{N_0 + N_2\sqrt{C_n} + N_3 C_n + N_4 C_n^{3/2} + N_5 C_n^2}}, \tag{5.10}$$

with $N_0 = \kappa^2\alpha'(\alpha - \alpha_1)/\alpha$, $N_1 = \alpha'(\alpha - \alpha_1)\kappa^2$, $N_2 = \kappa\alpha'(6 + \kappa\alpha)(\alpha - \alpha_1)/\alpha$, $N_3 = 3(\alpha - \alpha_1)[\alpha'(3 + 2\kappa\alpha) - 3\kappa^2]/\alpha$, $N_4 = 9\alpha'(\alpha - \alpha_1) - 3\kappa(1 - \alpha_1/\alpha) - 8\alpha\kappa^2 + 9\alpha_1\kappa^2$ and $N_5 = 3\alpha_1\kappa$. Numerically, we have

$$Fr_c = 0.373\sqrt{\frac{0.801 + 6.35\sqrt{C_n}}{0.0278 + 0.638\sqrt{C_n} + 3.72C_n + 3.57C_n^{3/2} + 1.90C_n^2}}. \tag{5.11}$$

Since the limit of C_n when $Re \to \infty$ is 0, it follows that the limit of Fr_c when $Re \to \infty$ is 2. However, the practical value of Fr_c is significantly smaller than 2. As C_n depends only on Re, Fr_c can be plotted as a function of the Reynolds number (figure 6*b*). For usual values of Re, the critical Froude number Fr_c is not far from the value given by the Gauckler–Manning–Strickler law. It can be as low as 1.4 for $Re \sim 10^4$ though.

5.3. *Total head, shape factors, momentum and energy slopes*

The total head is usually defined as $\mathcal{H} = Z + h\cos\theta + U^2/(2g)$ where Z is the bottom elevation from a horizontal datum. This definition is appropriate to the Saint-Venant equations from which it can be proved from the momentum equation that the difference in a steady flow between the head $\mathcal{H}_2$ at the abscissa x_2 of the channel and the head $\mathcal{H}_1$ at the abscissa x_1 satisfies the relation

$$\mathcal{H}_2 - \mathcal{H}_1 = -\int_{x_1}^{x_2} \frac{\tau_{xz}(0)}{\rho g h}\,\mathrm{d}x. \tag{5.12}$$

https://doi.org/10.1017/jfm.2017.626 Published online by Cambridge University Press

This means that the head loss is due to the bottom friction. Starting from the energy equation, this difference is

$$\mathcal{H}_2 - \mathcal{H}_1 = -\int_{x_1}^{x_2} \frac{W}{\rho g h U}\,\mathrm{d}x, \tag{5.13}$$

which implies that the head loss is due to the energy dissipation. The quantity $\tau_{xz}(0)/(\rho g h)$ is the momentum resistance slope or friction slope and $W/(\rho g h U)$ is the energy slope (Yen 1973, 2002). However, at $O(\mu^0)$ which is the order of approximation of the Saint-Venant equations, both quantities are equal.

Shearing effects are sometimes taken into account in the Saint-Venant model by the so-called shape factors: the Boussinesq coefficient $\beta_B = \langle u^2\rangle/U^2$ and the Coriolis coefficient $\alpha_C = \langle u^3\rangle/U^3$. Taking these coefficients constant, the momentum equation yields, in the stationary case (Chow 1959, p. 51)

$$\beta_B \frac{U_2^2}{2g} + h_2\cos\theta + Z_2 = \beta_B \frac{U_1^2}{2g} + h_1\cos\theta + Z_1 - \int_{x_1}^{x_2} \frac{\tau_{xz}(0)}{\rho g h}\,\mathrm{d}x, \tag{5.14}$$

whereas the energy equation implies (Chow 1959, p. 40)

$$\alpha_C \frac{U_2^2}{2g} + h_2\cos\theta + Z_2 = \alpha_C \frac{U_1^2}{2g} + h_1\cos\theta + Z_1 - \int_{x_1}^{x_2} \frac{W}{\rho g h U}\,\mathrm{d}x. \tag{5.15}$$

If the friction slope and the energy slope are supposed to be equal, then $\beta_B = \alpha_C$. This can happen only if both coefficients are equal to 1. It is thus inconsistent to include a deviation of the velocity profile from flatness without difference between the friction slope and the energy slope, or *vice versa*. If the friction slope and the energy slopes are distinguished, then there are three independent equations: two variables are not sufficient. The shape factors could be treated as variables but evolution equations should be provided for them.

We would rather consider the enstrophy and $\langle u^{*3}\rangle$. The latter was shown to be negligible in the approximation of weakly sheared flows. For the three-equation model (4.53)–(4.55), an appropriate total head is defined by

$$\mathcal{H} = \frac{U^2}{2g} + \frac{3h^2\varphi}{2g} + h\cos\theta + Z. \tag{5.16}$$

The head loss for steady flows can then be derived from the energy equation (and not from the momentum equation) with the relation (5.13) where the relevant slope is the energy slope (and not the friction slope). If needed, the shape factors can be calculated with $\beta_B = 1 + h^2\varphi/U^2$ and, in the approximation of weakly sheared flows, $\alpha_C = 1 + 3h^2\varphi/U^2$. The shape factors of the normal flow can be calculated consistently at order zero. The expression of the normal (equilibrium) Boussinesq coefficient is

$$\beta_n = 1 + \frac{C_n}{\alpha'}. \tag{5.17}$$

With Teshukov's approximation of weakly sheared flows, the expression of the normal Coriolis coefficient is

$$\alpha_n \simeq 1 + 3\frac{C_n}{\alpha'}. \tag{5.18}$$

https://doi.org/10.1017/jfm.2017.626 Published online by Cambridge University Press

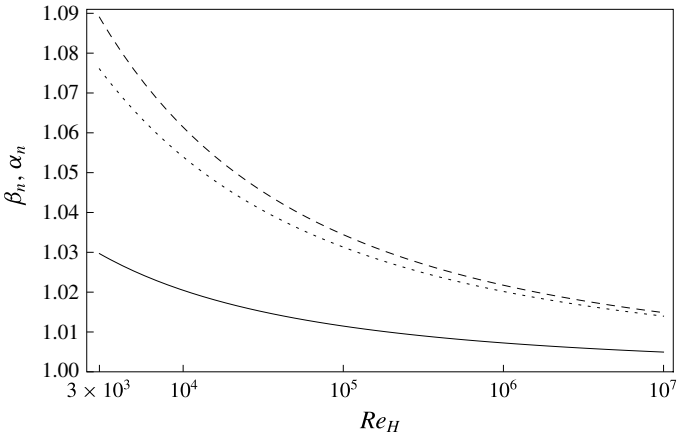


FIGURE 7. Variations of the normal Boussinesq shape factor β_n (solid curve), the normal Coriolis shape factor α_n (dotted curve) and the normal Coriolis shape factor in Teshukov's approximation of weakly sheared flows (dashed curve) as a function of the Reynolds number.

However, it is possible to calculate the normal Coriolis coefficient without Teshukov's approximation of weakly sheared flows. The full expression is

$$\alpha_n = 1 + 3\frac{C_n}{\alpha'} + \frac{C_n^{3/2}}{\kappa^3}\left(\frac{172}{135} - \frac{2}{3}\pi^2 + \frac{16}{3}\ln 2\right). \tag{5.19}$$

Since C_n depends only on the Reynolds number, α_n and β_n depend also only on the Reynolds number (figure 7). For $Re_H = 10^5$, $\beta_n - 1 \simeq 1.15 \times 10^{-2}$ and $\alpha_n - 1 \simeq 3.13 \times 10^{-2}$. Note that Teshukov's approximation of weakly sheared flows changes the numerical value of α_n by only 0.3 % (1.034 instead of 1.031) and the numerical value of $(\alpha_n - 1)$ by 10 % (3.44×10^{-2} instead of 3.13×10^{-2}).

5.4. *Backwater curves*

The nonlinear structure of the equations is now tested in the stationary case. In this case, the Saint-Venant equations reduced to the gradually varied flow equation, also called the backwater equation. For a steady flow, the flow rate $q = hU$ is constant. Denoting by h_c the critical depth (corresponding to a Froude number equal to 1), the backwater equation is (Chow 1959, p. 222)

$$\frac{\mathrm{d}h}{\mathrm{d}x} = S_0 \frac{1 - (h_n/h)^3}{1 - (h_c/h)^3}, \tag{5.20}$$

where S_0 is the channel slope which, in our notations, is equal to $\mathrm{tg}\theta$. The solution of this equation is the flow profile which is often called a backwater curve (although the term drawdown curve is sometimes used if the depth decreases in the direction of the flow, see Chow 1959, p. 222). If $h_n > h_c$ the slope is mild, and the backwater curves are called M1 if $h > h_n$, M2 if $h_c < h < h_n$ and M3 if $h < h_c$. If $h_n < h_c$ the slope is steep. The corresponding backwater curves are called S1 ($h > h_c$), S2 ($h_n < h < h_c$) and S3 ($h < h_n$). The slope is critical if $h_n = h_c$ and the backwater curves are C1 ($h > h_n$),

https://doi.org/10.1017/jfm.2017.626 Published online by Cambridge University Press

C3 ($h < h_n$) and C2 ($h = h_n$) (although C2 is a disputed case). The case of a horizontal slope or a negative (adverse) slope will not be considered here because there is no normal (equilibrium) flow in these two cases. Additionally, the flow is subcritical if $h > h_c$ and supercritical if $h < h_c$. For more details on the backwater curves, see Chow (1959). To calculate the backwater curves, equation (5.20) is solved with the adequate boundary conditions: upstream of the computation domain if the flow is supercritical, and downstream of it when the flow is subcritical. The computed backwater curve depends on the choice of the law for the friction factor.

Let us now see what happens if the three-equation model is used instead of the Saint-Venant equations. The system (with (4.58) instead of the energy equation) is written in the stationary case. The mass equation gives the conservation of the flow discharge q. The momentum equation becomes

$$\frac{\mathrm{d}h}{\mathrm{d}x} = \frac{K_1(gh\sin\theta - C_f q^2/h^2) + K_2(\alpha' h^2\varphi - gh\sin\theta)}{gh\cos\theta + 3h^2\varphi - q^2/h^2}, \tag{5.21}$$

where

$$K_1 = 1 + (2\alpha - 3\alpha_1)\sqrt{C_f}, \quad K_2 = \sqrt{C_f}[3(\alpha - \alpha_1) + \alpha(2\alpha - 3\alpha_1)\sqrt{C_f}]. \tag{5.22a,b}$$

And the stationary enstrophy equation reads

$$\frac{\mathrm{d}\varphi}{\mathrm{d}x} = -2(\alpha - \alpha_1)\frac{\sqrt{C_f}}{h^3}\left[gh\sin\theta - C_f\frac{q^2}{h^2} + (1 + \alpha\sqrt{C_f})(\alpha' h^2\varphi - gh\sin\theta)\right]. \tag{5.23}$$

These equations are put into dimensionless form with the following scaling:

$$X = \frac{x}{h_n}, \quad h' = \frac{h}{h_n}, \quad \varphi' = \frac{\varphi h_n}{Fr_n^2\, g\cos\theta}, \quad Fr_n^2 = \frac{q^2}{gh_n^3\cos\theta}. \tag{5.24a–d}$$

This leads to the dimensionless momentum equation

$$\frac{\mathrm{d}h'}{\mathrm{d}X} = \frac{K_1(\mathrm{tg}\theta - C_f Fr_n^2/h'^3) + K_2(\alpha' Fr_n^2 h'\varphi' - \mathrm{tg}\theta)}{1 + 3Fr_n^2 h'\varphi' - Fr_n^2/h'^3}, \tag{5.25}$$

and to the dimensionless enstrophy equation

$$\frac{\mathrm{d}\varphi'}{\mathrm{d}X} = -2(\alpha - \alpha_1)\frac{\sqrt{C_f}}{Fr_n^2 h'^2}\left[\mathrm{tg}\theta - C_f\frac{Fr_n^2}{h'^3} + (1 + \alpha\sqrt{C_f})(\alpha' Fr_n^2 h'\varphi' - \mathrm{tg}\theta)\right]. \tag{5.26}$$

The flow profile is calculated by solving this system (5.25)–(5.26). The treatment of the boundary conditions also differs from the Saint-Venant model. In the Saint-Venant model, there are two characteristic velocities $U - c$ and $U + c$ where $c = \sqrt{gh\cos\theta}$. If $U > c$ (supercritical case) the boundary conditions have to be chosen upstream of the computation domain: no wave can go upstream. If $U < c$ (subcritical case), the boundary conditions are chosen downstream. In the three-equation model, c has a different expression ($c = \sqrt{gh\cos\theta + 3h^2\varphi}$) but the main difference lies in the fact that there is a third characteristic U (see (5.3)). This characteristic corresponds

https://doi.org/10.1017/jfm.2017.626 Published online by Cambridge University Press

to the advection of the enstrophy. Consequently, the boundary condition for the enstrophy must always be taken upstream of the computation domain. The second boundary condition must also be taken upstream if the flow is supercritical ($U > c$ with the new expression of c). In this case, both boundary conditions can be taken at the same upstream point. If, on the contrary, the flow is subcritical, the second boundary condition is taken downstream of the computation domain. This means that the resolution of the problem is no longer a Cauchy problem (i.e. an initial value problem) but a boundary value problem. To solve these cases, a shooting method was used.

The calculated flow profiles are very similar to those calculated with the backwater equation (5.20) and these profiles will also be called backwater curves with the same classification for the mild and steep slopes (M1, M2, S1, etc.). The computation of the backwater curve with the three-equation model can be made much easier with the following approximation: the right-hand side of the enstrophy equation (5.26) is almost equal to zero everywhere except close from the critical depth. If the derivative $\mathrm{d}\varphi'/\mathrm{d}X$ is taken equal to zero, then the enstrophy can be expressed as a function of the depth h' as

$$\varphi'^{*} = \frac{\sqrt{C_f}}{\alpha'(1+\alpha\sqrt{C_f})}\left(\frac{\alpha \mathrm{tg}\theta}{Fr_n^2 h'} + \frac{\sqrt{C_f}}{h'^4}\right). \tag{5.27}$$

If $\varphi' = \varphi'^{*}$, then the momentum equation (5.25) takes the simplified form

$$\frac{\mathrm{d}h'}{\mathrm{d}X} = \mathrm{tg}\theta \frac{1 - C_f/(C_n h'^3)}{1-(h'_c/h')^3} \frac{1}{1+\alpha\sqrt{C_f}(1+3\mathrm{tg}\theta/\alpha')}, \tag{5.28}$$

where h'_c is the dimensionless critical depth corresponding to $Te = 1$. This expression is very similar to the usual backwater equation (5.20) with the following difference: the friction factor C_f is a variable and thus is not always equal to its normal value C_n, which means that the numerator is not simply $1 - h'^{-3}$, and the slope is divided by $1+\alpha\sqrt{C_f}(1+3\mathrm{tg}\theta/\alpha')$. The usual backwater curve is formally recovered by taking $\alpha = 0$ and $C_f = C_n$.

The approximation $\varphi' \simeq \varphi'^{*}$ is valid if $|\partial h'/\partial X|$ is very small, which happens everywhere except close to the critical depth or for backwater curves of short lengths. With this approximation, the computation of the subcritical backwater curves can be done as easily as in hydraulics, taking the depth boundary condition at the downstream control section and calculating upstream.

The M1 backwater curve for $Re_H = 10^5$, $C_n = 0.00249$, $Fr_n = 0.2$ and $\mathrm{tg}\theta = 10^{-4}$ is presented in figure 8. At the upstream control section, φ' is set to the value φ'^{*} which in this case is equal to φ_n since the M1 curve tends asymptotically towards the normal depth when going upstream. At the downstream control section, the depth is fixed to the value $h'(X = 40\,000) = 2.2$. The calculation was done with a shooting method. This calculation can also be done with the downstream boundary condition only, with the approximation $\varphi' = \varphi'^{*}$, with an accuracy better than 0.033 %. This approximation gives very accurate results here because this backwater curve is very long and $|\partial h'/\partial X|$ very small.

The relative difference between the depth profile calculated with the three-equation model and with the Saint-Venant model depends very little on the choice of the friction law used in the Saint-Venant equations (see figure 8*a*). This difference can be greater than 10 % whatever the friction law used (figure 8*b*) and seems to be

https://doi.org/10.1017/jfm.2017.626 Published online by Cambridge University Press

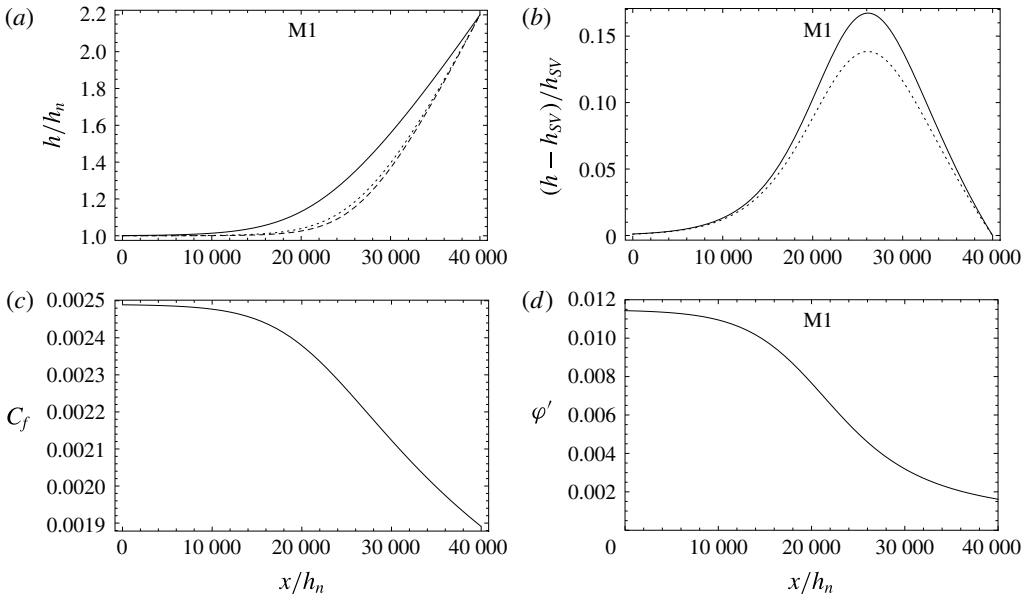


FIGURE 8. The M1 backwater curve: (*a*) depth profile (solid curve: three-equation model; dashed curve: Saint-Venant model with the same friction law (4.41); dotted curve: Saint-Venant model with $C_f = C_n$); (*b*) relative deviation from the Saint-Venant model with friction law (4.41) (solid curve) or with $C_f = C_n$ (dotted curve); (*c*) friction factor; (*d*) enstrophy profile.

measurable experimentally. It would be interesting to check whether experiments confirm or not this deviation from the Saint-Venant backwater curve. The friction factor (figure 8*c*) and the enstrophy (figure 8*d*) decrease markedly when going downstream.

The backwater curves calculated with the three-equation model can be significantly different from those calculated with the Saint-Venant model, whatever the friction law, for high depth curves (M1 and S1) whereas no firm conclusion can be drawn for the small depth curves (M3 and S3) because the dependence of the Saint-Venant backwater curves towards the friction law is so high. In the case of the M2 and S2 curves, a significant deviation can sometimes be found.

5.5. *Roll waves*

System (4.53)–(4.55) having the hyperbolic structure of the compressible Euler equations with relaxation source terms, classical numerical schemes can be used. These schemes are well known to be robust, reliable and easy to implement. Denoting by $\overline{\boldsymbol{U}} = [h, hU, he]^{\mathrm{T}}$ the matrix of the conservative variables, by $\overline{\boldsymbol{F}} = [hU, hU^2 + P, hU(e + P/h)]^{\mathrm{T}}$ the matrix of the fluxes and by $\overline{\boldsymbol{S}}$ the matrix of the source terms

$$\begin{bmatrix} 0 \\ (1-\alpha_1\sqrt{C_f})(gh\sin\theta - C_f U|U|) + (\alpha - \alpha_1 - \alpha\alpha_1\sqrt{C_f})\sqrt{C_f}(\alpha' h^2\varphi - gh\sin\theta) \\ (1-\alpha\sqrt{C_f})(gh\sin\theta - C_f U|U|)U - \alpha^2 C_f(\alpha' h^2\varphi - gh\sin\theta)U \end{bmatrix}, \tag{5.29}$$

https://doi.org/10.1017/jfm.2017.626 Published online by Cambridge University Press

the equations can be written

$$\frac{\partial \overline{\boldsymbol{U}}}{\partial t} + \frac{\partial \overline{\boldsymbol{F}}}{\partial x} = \overline{\boldsymbol{S}}. \tag{5.30}$$

The friction factor $C_f = f/8$ follows the law (4.41). These equations are discretized by a classical Godunov finite-volume method, as

$$\overline{\boldsymbol{U}}_i^{n+1} = \overline{\boldsymbol{U}}_i^n + \frac{\Delta t}{\Delta x}(\overline{\boldsymbol{F}}_{i-1/2}^n - \overline{\boldsymbol{F}}_{i+1/2}^n) + \overline{\boldsymbol{S}}_i^n \Delta t, \tag{5.31}$$

where Δt is the time step and Δx the cell width. In this expression, $\overline{\boldsymbol{X}}_j^n$ is the matrix $\overline{\boldsymbol{X}}$ in cell j and at iteration n. The fluxes $\overline{\boldsymbol{F}}_{i-1/2}^n$ and $\overline{\boldsymbol{F}}_{i+1/2}^n$ denote the intercell fluxes. They are computed with the approximate Riemann solver, which is either the Rusanov method or the HLLC (Harten, Lax, Van Lear, Contact) method. A second-order scheme was obtained with the monotone upstream-centred scheme for conservation laws (MUSCL) method coupled with the Heun method.

This numerical scheme was used to calculate roll waves. The experimental conditions of Brock (1967) are simulated with a HLLC solver, a second-order scheme and a Courant–Friedrichs–Levy (CFL) number equal to 0.5. The flow being always supercritical, the depth, discharge and enstrophy are imposed at the entrance of the channel and the variables in the last cell are taken as equal to those of the penultimate cell. The initial conditions are the values of the normal flow. At the entrance, a sinusoidal perturbation on the depth is applied with an amplitude equal to 3 % of the normal depth and a period T. The entrance enstrophy and discharge are fixed at the normal value.

The width of the channel used by Brock (1967) was $\ell = 11.75$ cm. Consequently, there is a small discrepancy between the experiments and the purely one-dimensional theoretical problem that is studied here. In particular, there is a difference between the normal fluid depth h_n and the hydraulic radius $r = \ell h_n/(\ell + 2h_n)$. We chose to keep the values of the slope, of the normal depth h_n, of the normal velocity U_n and of the normal Froude number Fr_n of the experiments. The normal friction factor $C_n = gh_n \sin\theta/U_n^2$ is thus fixed to a value slightly different from Brock (1967) where it was calculated by $gr \sin\theta/U_n^2$. Then the Reynolds number Re_H is calculated with relation (4.39) and is different from the Reynolds number of the experiments. Finally, the kinematic viscosity is calculated by $\nu = 4h_nU_n/Re_H$. Its numerical value is not the value expected from the experiments' temperature.

As the comparisons with all experiments of Brock on periodic waves on a smooth bottom give the same trend, only one case is presented in this paper. This case is numbered case 9 in Richard & Gavrilyuk (2012). The parameters of the calculation are: $h_n = 5.33$ mm; $U_n = 1.28$ m s^{-1}; tg$\theta = 0.1201$; $Fr_n = 5.622$ ($F_n = 5.60$); $T = 1.016$ s. The length of the channel is $L = 24.4$ m. All these values are identical to the values measured by Brock. The normal friction factor is $C_n = 0.0038$ (instead of 0.0035 in Brock's experiments) and the Reynolds number is $Re_H = 1.755 \times 10^4$ (instead of 2.60×10^4). The kinematic viscosity is $\nu = 1.556 \times 10^{-6}$ m^2 s^{-1} which corresponds to a temperature of 4 °C (instead of the temperature of 22 °C of the experiments which gives a kinematic viscosity of $\nu = 0.957 \times 10^{-6}$ m^2 s^{-1}).

The results are presented in figure 9. The uniform flow being unstable, the inlet perturbation produces waves that grow, steepen and finally break (figure 9*a*). The waves breaking is easily detected by the appearance of a very sharp peak of enstrophy at the wave front (figure 9*b*). Apart from this peak, the enstrophy is not constant. It is smaller when the depth is higher and *vice versa*. This is easily explainable since there

https://doi.org/10.1017/jfm.2017.626 Published online by Cambridge University Press

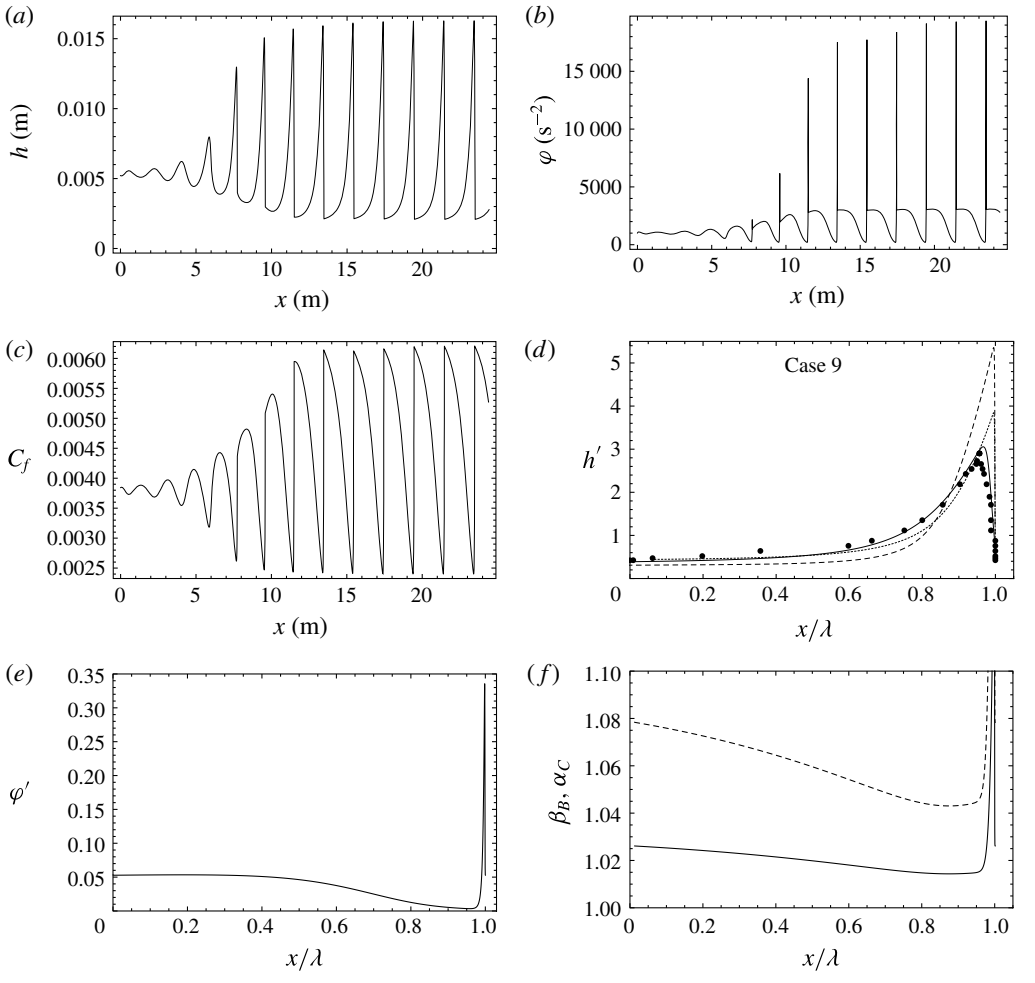


FIGURE 9. Roll waves: (*a*) depth profile on the whole channel; (*b*) enstrophy profile; (*c*) friction factor variation in the channel; (*d*) dimensionless depth profile in one wavelength: three-equation model (solid curve); Saint-Venant solution with $C_f = C_n$ (dotted curve); Saint-Venant solution with law (4.41) (dashed curve); experimental measurements of Brock (1967) (dots); (*e*) dimensionless enstrophy profile in one wavelength; (*f*) variation of the Boussinesq coefficient β_B (solid curve) and of the Coriolis coefficient α_C (dashed curve) in one wavelength.

is relatively more shearing if the depth is smaller. The friction factor varies strongly between a low value when the depth is high to a much higher value when the depth is shallow (figure 9*c*). After some distance (that is here less than 20 m), a periodic regime of roll waves is reached. The variations of the dimensionless depth $h' = h/h_n$, the dimensionless enstrophy and the shape factors in one period are shown in 9(*d*), (*e*) and (*f*) respectively. The dimensionless abscissa is x/λ where x is the abscissa and λ the wavelength measured by Brock (1967). There is a very sharp peak of the values of the shape factors in the region of the wave front. The Boussinesq coefficient reaches a value of 1.22 and the peak value of the Coriolis coefficient is 1.66. Apart from this peak, the variations of these factors are more moderate (figure 9*f*). Assuming a

https://doi.org/10.1017/jfm.2017.626 Published online by Cambridge University Press

	c (m s^{-1})	λ (m)	$\Delta\lambda/\lambda$	h'_{max}	h'_{min}	a'	$\Delta a'/a'_B$	$\Delta e/e_B$
Brock (1967)	2.00	2.03	0	2.91	0.43	2.48	0	0
3 eq. model	1.98	2.01	−1.1 %	3.06	0.39	2.66	+7.4 %	−24 %
SV C_n	1.89	1.92	−5.7 %	3.84	0.44	3.40	+37 %	−100 %
SV var.	2.17	2.20	+8.3 %	5.36	0.31	5.05	+104 %	−100 %

TABLE 1. Numerical results for periodic roll waves.

constant value for the shape factors is thus totally unrealistic if rollers appear in the flow, as it was pointed out by Kranenburg (1992).

The depth variation is compared to the experimental points of Brock (1967) and to the results given by the numerical resolution of the Saint-Venant equations in two cases: the friction factor is calculated by the law (4.41) or the friction factor is constant and equal to its normal value C_n. The results are presented in table 1. The temporal period is exactly the same as in Brock's experiments. The calculated wave velocity and wavelength are 1.1 % less than the measured values. By comparison, the Saint-Venant model with constant friction factor gives values 5.7 % smaller than the measurements and the Saint-Venant model with the friction law (4.41) gives results 8.3 % higher than the measured values. The calculated wave amplitude defined by $a' = h'_{max} - h'_{min}$, where h'_{max} and h'_{min} are respectively the maximum and minimum dimensionless depths, is overestimated by 7.4 %. This is much better than the amplitude calculated with the Saint-Venant equations which is 37 % higher with a constant friction factor and 104 % higher with a variable friction factor. The shock thickness is defined by the distance between the wave front and the maximum depth position. Its calculated value is underestimated by 24 %. With the Saint-Venant equations, this shock thickness is equal to zero (−100 %) since the periodic roll waves solutions (Dressler 1949) have a depth discontinuity between the minimum depth and the maximum depth and a monotone continuous depth profile between these discontinuities.

The waves celerity (c), the wavelength (λ), the relative deviation of the wavelength from the experimental value $\Delta\lambda/\lambda$, the maximum depth, the minimum depth, the wave amplitude, the relative deviation of the amplitude from the experimental value a'_B, the relative deviation on the shock thickness e from the experimental value e_B are given in table 1 for the experiments of Brock (1967), the three-equation model (3 eq. model), the Saint-Venant model with $C_f = C_n$ (SV C_n) and the Saint-Venant model with law (4.41) (SV var.). The three-equation model gives much better results than the Saint-Venant model and is in reasonable agreement with the experimental measurements of Brock (1967). Of course, models with an empirical law and adjustable parameters fitted to Brock's measurements like in Richard & Gavrilyuk (2012) or Cao *et al.* (2015) give more precise results but the three-equation model presented in this paper has zero adjustable parameter and no *ad hoc* law specially designed for roll waves. Note that the Saint-Venant model with $C_f = C_n$ is clearly better than the Saint-Venant model with the consistent law (4.41). This effect is also observed for some backwater curves but it is here more pronounced.

6. Conclusion

We derived a three-equation model for the hydraulics of open-channel flows in the smooth turbulent regime. This model is an extension of the Saint-Venant model which

https://doi.org/10.1017/jfm.2017.626 Published online by Cambridge University Press

is recovered at a certain order of approximation. Starting from a turbulence model of mixing length and from the matching of two asymptotic expansions in a shallow-water layer and a viscous layer near to the bottom, the model provides a consistent description of weakly sheared flows. It features equations for mass, momentum and energy balances and has the hyperbolic structure of the compressible Euler equations with relaxation source terms. It includes every terms of the Saint-Venant equations and adds corrective terms that depends only on the friction factor for which a law similar to the Colebrook–White relation restricted to smooth bottoms is consistently derived.

Shearing effects are included through a variable called enstrophy which is of the order of $O(\mu^2)$ where $\mu = 2/\ln(\kappa^2 Re)$. The approximation of weakly sheared flows amounts to neglect terms of $O(\mu^3)$. We want to emphasize that the Saint-Venant equations with a negligible deviation to a flat velocity profile and a friction term are a consistent model of $O(\mu^0)$. The traditional approach in hydraulics of open-channel flows which includes friction but no deviation of the velocity profile from flatness is wholly legitimate. We showed that taking into account a non-flat velocity profile, i.e. at $O(\mu^2)$, entails additional terms to the usual Saint-Venant equations with friction. Moreover, at $O(\mu^2)$, the energy equation becomes independent of the momentum equation as the dissipation power in the energy equation is not equal to the power of the friction force that appears in the momentum equation. More precisely, the dissipation power is not equal to the product of the friction force with the average fluid velocity if the deviation of the velocity profile to a flat profile is not neglected. The model allows us to calculate the Boussinesq and Coriolis shape factors but the independence of the energy equation from the momentum equation not only legitimates but requires the introduction of a third variable which, in the present model, is the enstrophy.

Due to its simple mathematical structure (hyperbolic, in conservative form), the new system is easily solved with classical finite volume numerical schemes, that can handle possible discontinuities. The friction factor is calculated by a local law, depending only on the kinematic viscosity, the slope and on the local fluid depth.

As for the Saint-Venant model, the backwater curves can be computed by restricting the equations of the model to the stationary case. For supercritical flows, these curves are calculated starting from an upstream control and going downstream, as in classical hydraulics. For subcritical flows, the calculation of the backwater curves is not an initial value problem but a boundary value problem because the enstrophy is always advected downstream. In many cases, however, this situation can be simplified with an approximation on the calculation of the enstrophy allowing to calculate the backwater curves from a downstream control and going upstream.

The model was applied to calculate the critical Froude number above which a uniform flow becomes unstable. The velocity of the kinematic waves was also calculated, as a function of the Reynolds number. Its value is close to the value given by the empirical law of Gauckler–Manning–Strickler. The backwater curves were found to be similar to the usual backwater curves calculated with the Saint-Venant equations but a significant difference was noticed in some cases, particularly for the M1 backwater curves. The growth, steepening and breaking of roll waves can be easily calculated as well as the periodic waves. The numerical results are in fair agreement with the experiments of Brock (1967) and are much better than the roll waves calculated with the Saint-Venant equations in all respects: wavelength, wave velocity, wave amplitude, depth profile and shock thickness.

It is worth noting that the consistent writing of the Saint-Venant equations with friction implies to use the same friction law as for the three-equation model, which

https://doi.org/10.1017/jfm.2017.626 Published online by Cambridge University Press

is related to the Colebrook–White relation for smooth walls. But we showed that, if the Saint-Venant equations are to be used, the results are often significantly improved by using instead a constant friction factor equal to the friction factor calculated for the steady uniform flow even in the case of a variable flow. This justifies a common practice in hydraulics of open-channel flows. On the other hand, assuming a constant friction factor underestimates significantly the velocity of the kinematic waves.

Since this three-equation model has no empirical law nor adjustable parameter designed to handle specifically some particular phenomena, it has the same universal nature as the Saint-Venant equations to which it adds corrective terms. It could be helpful in hydraulic of open-channel flows in case a greater precision is needed. The expected developments of this work include the extension to a rough bottom, to a variable bottom and a two-dimensional model. Also the corrective terms on the wall friction could have an effect on the evolution of erodible beds, in the spirit of Luchini & Charru (2010*b*).

Acknowledgements

The work was supported by the Service Hydrographique et Océanographique de la Marine (SHOM). A.R. thanks the Fondecyt project 11130378.

Supplementary material

A supplementary document detailing the long calculations of § 3.3 is available at https://doi.org/10.1017/jfm.2017.626.

Appendix A. Error estimation on the integral R

We estimate here the error made when R is substituted to the integral $\mathcal{R}(Mb/\sqrt{\eta})$ in the matching procedure. Let

$$E(Z) = \frac{1}{1+\sqrt{1+Z^2(1-\mathrm{e}^{-Z/A})^2}} - \frac{1}{1+\sqrt{1+Z^2}}, \tag{A 1}$$

so that

$$R - \mathcal{R}(Mb\eta^{-1/2}) = \int_{Mb\eta^{-1/2}}^{+\infty} E(Z)\,\mathrm{d}Z. \tag{A 2}$$

Rewriting $E(Z)$ as

$$\frac{2Z^2\mathrm{e}^{-Z/A}(1-\mathrm{e}^{-Z/A}/2)}{(1+\sqrt{1+Z^2(1-\mathrm{e}^{-Z/A})^2})(1+\sqrt{1+Z^2})(\sqrt{1+Z^2}+\sqrt{1+Z^2(1-\mathrm{e}^{-Z/A})^2})}, \tag{A 3}$$

we obtain, since $\sqrt{1+Z^2(1-\mathrm{e}^{-Z/A})^2} \geqslant 1$,

$$E(Z) \leqslant \frac{Z^2\mathrm{e}^{-Z/A}(1-\mathrm{e}^{-Z/A}/2)}{(1+\sqrt{1+Z^2})^2} \leqslant \mathrm{e}^{-Z/A}. \tag{A 4}$$

Consequently,

$$|R - \mathcal{R}(Mb\eta^{-1/2})| \leqslant A\mathrm{e}^{-Mb\eta^{-1/2}/A}. \tag{A 5}$$

https://doi.org/10.1017/jfm.2017.626 Published online by Cambridge University Press

Since $\eta = \varepsilon^{2+m}$ with $m > 0$ and because

$$\forall n > 0, \quad \forall m > 0, \quad \lim_{\varepsilon \to 0^+} \left[\varepsilon^{-n} \exp\left(-\frac{1}{\sqrt{\varepsilon^{2+m}}} \right) \right] = 0, \tag{A 6}$$

we get, for all $n > 0$, $R - \mathcal{R}(Mb\eta^{-1/2}) = O(\varepsilon^n)$. Consequently, the error made by replacing $\mathcal{R}(Mb/\sqrt{\eta})$ with R is negligible. The proof of the smallness of the difference between $\mathcal{R}_1(Mb/\sqrt{\eta})$ and R_1 is done similarly, replacing the function E by E_1:

$$E_1(Z) = \frac{1}{\sqrt{1 + Z^2(1 - \mathrm{e}^{-Z/A})^2}} - \frac{1}{\sqrt{1 + Z^2}}, \tag{A 7}$$

and controlling it with $E_1(Z) \leqslant 2\exp(-Z/A)$.

REFERENCES

BAILEY, S. C. C., VALLIKIVI, M., HULTMARK, M. & SMITS, A. J. 2014 Estimating the value of von Kármán's constant in turbulent pipe flow. *J. Fluid Mech.* **749**, 79–98.

BARRÉ DE SAINT-VENANT, A. J. C. 1871 Théorie et équations générales du mouvement non permanent des eaux courantes. *C. R. Acad. Sci.* **73**, 147–154.

BROCK, R. R. 1966 Discussion. *J. Hydraul. Div.* **92**, 403–409.

BROCK, R. R. 1967 Development of roll waves in open channels. PhD thesis, California Institute of Technology.

CAO, Z., HU, P., HU, K., PENDER, G. & LIU, Q. 2015 Modelling roll waves with shallow water equations and turbulent closure. *J. Hydraul. Res.* **53** (2), 161–177.

CHOW, V. T. 1959 *Open Channel Hydraulics*. McGraw-Hill.

COUSTEIX, J. & MAUSS, J. 2004 Approximations of the Navier–Stokes equations for high Reynolds number flows past a solid wall. *J. Comput. Appl. Maths* **166** (1), 101–122.

COUSTEIX, J. & MAUSS, J. 2007 *Asymptotic Analysis and Boundary Layers*. Springer.

DARCY, H. 1854 Sur des recherches expérimentales relatives au mouvement des eaux dans les tuyaux. *C. R. Acad. Sci.* **38**, 1109–1121.

D'AUBUISSON DE VOISINS, J. F. 1840 *Traité d'hydraulique*. Levraut.

DECOENE, A., BONAVENTURA, L., MIGLIO, E. & SALERI, F. 2009 Asymptotic derivation of the section-averaged shallow water equations for natural river hydraulics. *Math. Models Meth. Appl. Sci.* **19** (3), 387–417.

DRESSLER, R. F. 1949 Mathematical solution of the problem of roll-waves in inclined open channels. *Commun. Pure Appl. Maths* **2** (2–3), 149–194.

GAUCKLER, P. 1868 Du mouvement de l'eau dans les conduites. *Ann. des Ponts et Chaussées* **15** (4), 229–281.

HENDERSON, F. M. 1996 *Open Channel Flow*. Macmillan.

KRANENBURG, C. 1992 On the evolution of roll waves. *J. Fluid Mech.* **245**, 249–261.

LUCHINI, P. & CHARRU, F. 2010*a* Consistent section-averaged equations of quasi-one-dimensional laminar flow. *J. Fluid Mech.* **656**, 337–341.

LUCHINI, P. & CHARRU, F. 2010*b* The phase lead of shear stress in shallow-water flow over a perturbed bottom. *J. Fluid Mech.* **665**, 516–539.

MANNING, R. 1895 On the flow of water in open channels and pipes. *Trans. Inst. Civil Eng. Ireland* **20**, 161–207.

MELLOR, G. L. 1972 The large Reynolds number, asymptotic theory of turbulent boundary layers. *Intl J. Engng Sci.* **10**, 851–873.

NOBLE, P. & VILA, J.-P. 2013 Thin power-law film flow down an inclined plane: consistent shallow-water models and stability under large-scale perturbations. *J. Fluid Mech.* **735**, 29–60.

POULIQUEN, O. 1999 Scaling laws in granular flows down rough inclined planes. *Phys. Fluids* **11** (3), 542–548.

https://doi.org/10.1017/jfm.2017.626 Published online by Cambridge University Press

POULIQUEN, O. & FORTERRE, Y. 2002 Friction law for dense granular flows: application to the motion of a mass down a rough inclined plane. *J. Fluid Mech.* **453**, 133–151.

RICHARD, G. L. 2013 Élaboration d'un modèle d'écoulements turbulents en faible profondeur. Application au ressaut hydraulique et aux trains de rouleaux. PhD thesis, Université d'Aix-Marseille.

RICHARD, G. L. & GAVRILYUK, S. L. 2012 A new model of roll waves: comparison with Brock's experiments. *J. Fluid Mech.* **698**, 374–405.

RICHARD, G. L. & GAVRILYUK, S. L. 2013 The classical hydraulic jump in a model of shear shallow-water flows. *J. Fluid Mech.* **725**, 492–521.

RICHARD, G. L., RUYER-QUIL, C. & VILA, J. P. 2016 A three-equation model for thin films down an inclined plane. *J. Fluid Mech.* **804**, 162–200.

RUYER-QUIL, C. & MANNEVILLE, P. 2000 Improved modeling of flows down inclined planes. *Eur. Phys. J.* B **15** (2), 357–369.

SAVAGE, S. B. & HUTTER, K. 1989 The motion of a finite mass of granular material down a rough incline. *J. Fluid Mech.* **199**, 177–215.

STRICKLER, A. 1923 Beiträge zur Frage der Geschwindigkeitsformel und der Rauhigkeitszahlen für Ströme, Kanäle und geschlossene Leitungen. Mitteilungen des eidgenössischen Amtes für Wasserwirtschaft, **16**, Bern.

STURM, T. W. 2010 *Open Channel Hydraulics*. McGraw-Hill.

TESHUKOV, V. M. 2007 Gas-dynamics analogy for vortex-free boundary flows. *J. Appl. Mech. Tech. Phys.* **48** (3), 303–309.

THUAL, O. 2013 Modelling rollers for shallow water flows. *J. Fluid Mech.* **728**, 1–4.

TRACY, H. J. & LESTER, C. M. 1961 Resistance coefficients and velocity distribution in smooth rectangular channel. *Tech. Rep.* US Geological Survey.

USHA, R. & UMA, B. 2004 Modeling of stationary waves on a thin viscous film down an inclined plane at high Reynolds numbers and moderate Weber numbers using energy integral method. *Phys. Fluids* **16** (7), 2679–2696.

VAN DRIEST, E. R. 1951 Turbulent boundary layer in compressible fluids. *J. Aeronaut. Sci.* **18**, 145–160, 216.

VAN DRIEST, E. R. 1956 On turbulent flow near a wall. *J. Aeronaut. Sci.* **23**, 1007–1011.

VAN DRIEST, E. R. 1959 Convective heat transfer in gases. In *Turbulent Flows and Heat Transfer* (ed. C. C. Lin), pp. 339–427. Princeton University Press.

VAN DYKE, M. 1964 *Perturbation Methods in Fluid Mechanics*. Academic.

WEISBACH, J. 1845 *Lehrbuch der Ingenieur und Maschinenmechanik*. Brunswick.

YEN, B. C. 1973 Open-channel flow equations revisited. *J. Engng Mech. Div.* **99** (5), 979–1009.

YEN, B. C. 2002 Open channel flow resistance. *J. Hydraul. Engng* **128** (1), 20–39.

https://doi.org/10.1017/jfm.2017.626 Published online by Cambridge University Press